CAAP Final Report

Date of Report:	October 10, 2017
Contract Number:	DTPH56-14-S-N000006
Prepared for:	Government Agency: DOT
Project Title:	Laser peening for preventing pipe corrosion and failure
Prepared by:	Board of Regents of the University of Nebraska for the University of Nebraska-Lincoln

Contact Information: Yongfeng Lu
Lott Distinguished Professor
Department of Electrical and Computer Engineering,
University of Nebraska-Lincoln,
209N Walter Scott Engineering Center,
Lincoln, NE 68588-0511
Phone : (402)472 8323
E-mail : ylu2@unl.edu

Other members : Leimin Deng (Postdoctoral Researcher) ; Chenfei Zhang (Ph.D Student) ; Shiding Sun (Ph. D Student) ; Timothy Carlson (Undergraduate student).

Business and Activity Section

1. Major goal and objectives of the project

The ultimate goal of this project is to investigate and develop laser peening of stainless and carbon steels used for pipeline construction to improve their corrosion resistance. The corrosion resistance of pipelines will be enhanced via the compressive residual stress created by laser-induced shock waves during laser peening. It is anticipated that using laser shock peening in the construction of a pipeline will highly improve the reliability, safety, and lifespan of the nation's pipeline transportation system. As stated in our proposal, the major goals of this project will be achieved by organizing the project into four phases, each with specific objectives. Table 1 summarizes the final accomplishment of each phase and its objectives.

Table 1. The completion rate for the objectives of each phase of the project

Phases	Major Goals and Milestones	Starting Date (mm/dd/yy)	Ending Date (mm/dd/yy)	Completion Rate (%)
Phase 1	1) Develop experimental setup for laser cleaning.	10/01/2014	12/31/2014	100
	2) Establish cleaning mechanism and parameter windows.	01/01/2015	09/30/2016	100
	3) Develop real-time monitoring of cleaning process.	01/01/2015	09/30/2016	No need
Phase 2	1) Develop laser peening system.	10/01/2014	12/31/2014	100
	2) Establish parameter windows for laser peening.	01/01/2015	09/30/2016	100
Phase 3	1) Study surface morphology of the laser-peened surfaces.	01/01/2015	09/30/2016	100
	2) Determine residual stress of pipeline steels after laser cleaning and peening.	01/01/2015	09/30/2016	100
	3) Study corrosion resistance of laser-peened surface.	01/01/2015	09/30/2016	100
Phase 4	Design a laser peening prototype system.	06/30/2016	09/30/2016	100

2. *Significant results*

2.1. Experimental procedures

2.1.1. Material Preparation

In this report, the samples were prepared from 304 stainless steel (SS), 1018 carbon steel (CS), and Al-Mg alloy, which were cut into rectangular shapes with different dimensions for laser shock peening and related characterizations. Mechanical and electrochemical polishing was performed on sample surfaces, if needed, to obtain mirror-like surfaces. For mechanical polishing, sandpapers of different grades (400-1200 grits) were used. For electrochemical polishing, samples were immersed in a professional polishing solution ($HClO_4$: Ethanol, 1 : 9) with a positive bias of +25 V for certain time. Al-Mg alloys were used for preliminary tests since it is easy to be affected by laser shock peening.

2.1.2. Laser shock peening and laser cleaning

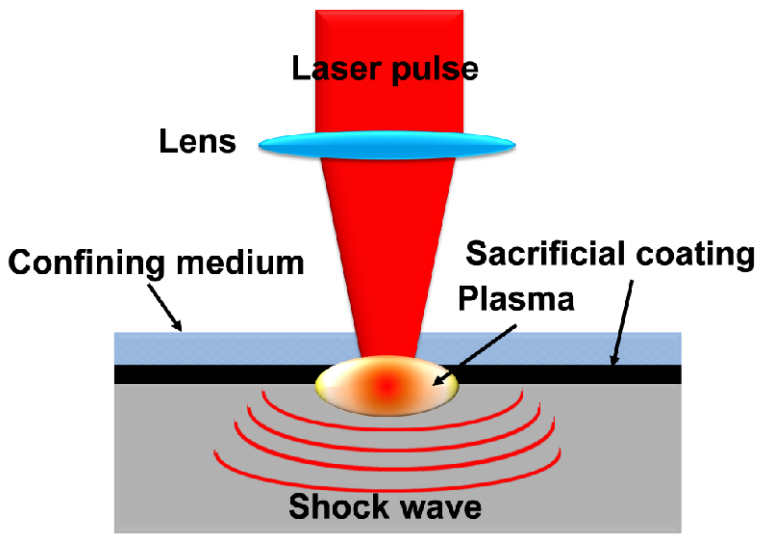

Fig. 1. Schematic of the principle of LSP.

Laser shock peening (LSP) is a cold mechanical process where pressure waves caused by expanding plasma plastically deform the surface of a material, as shown in Fig. 1. LSP uses a thin layer of ablative material that is opaque to the laser. The opaque ablative material, typically black spray paint or tape, is used as a sacrificial layer in the early study by Fairland and Clauer. The sacrificial layer also minimizes thermal effects on the surface caused by laser. The laser partially vaporizes the ablative layer to form high pressure plasma. The plasma, confined by a thin layer of water film (confining medium), expands rapidly resulting in a recoiling pressure wave on the order of GPa reported by Fariland et al. and Caslaru, et al. The pressure wave is cold mechanical process that typically deforms the surface. The plasma-induced shock pressure causes severe plastic deformation, refined grain size, compressive residual stresses, and

increased hardness at the surface and in the subsurface. As a result, the mechanical properties on the work-piece surface will be enhanced to improve the performance of corrosion and foreign objective damage.

In this project, the setup for LSP were modified for several times to improve peening effect and achieve portability. Therefore, the detailed setup description will be provided seperately in different sections. Laser cleaning always used the same setup as that of LSP.

2.1.3. Characterizations

Various analytical techniques were used for characterization of the samples before and after LSP for optimizing the LSP parameters. Optical microscopy (Nikon ECLIPSE, Japan) and electrical scanning microscopy (SEM, Philips, XL 30E, 5kV) were used to study the morphology of laser-peened samples. 3D profiler (New View 8000, Zygo Corporation) was used to measure the 3D profiles of the macro plastic deformation from the bottom surface of samples. The micromechanical properties were investigated on both the surfaces and cross sections of the tested samples using Hysitron TI 950 Triboindenter® with the standard three-sided pyramidal Berkovich (TI-00039) probe and Tukon 2500 Vickers & Knoop micro-hardness tester with the square-based diamond pyramid indenter. Residual stress measurements were conducted by X-ray diffraction (XRD) though Rigaku Smartlab with Cu as anode target. Monochrometer was used when 304 SS and 1018 CS were tested to reduce the influence of Cu peaks. In-depth residual stress investigations were carried out through electrochemical polishing and XRD layer by layer.

To perform metallographic observation, the surfaces and cross sections of the samples were etched to show up grain boundaries and different phases using specific reagent. For 304 SS, aqua regia (volume ratio of HCl to HNO_3: 3:1) was adopted; for 1018 CS, nital consisting of 4% HNO_3 and 96% ethanol was used. The etched surfaces of the samples were then investigated by optical microscope (OM, Nikon ECLIPSE, Japan), Keyence laser-scanning microscope (VK-X200K) and electron scanning microscope (SEM, Philips, XL 30E, 5kV).

In addition, the micro-structural changes in laser-peened sample surface were characterized using transmission electron microscope (TEM, JEOL 2010, Japan). The TEM samples were prepared by the following steps: (1) the front surface of the sample ($10\times10\times2$ mm^3) were firstly processed by large area laser peening for pre-determined times; (2) the processed samples were cut parallel to the laser-peened surface to decrease the sample thickness from 2 to approximately 1 mm; (3) the samples (front surface) were attached to the holder with superglue, grinded from the back face to decrease the sample thickness to about 150 μm and polished to mirror like surface with sand paper and polishing powder; (4) the samples were detached from the holder by ultrasonic with acetone and the back surface were attached to the holder to polish the front surface with polishing powder only; (5) the sample were detached from the holder and cleaned by ultrasonic

with acetone; (6) the thin slides were punched to get small wafers of the diameter of 3 mm; and (7) double-jet electro-polishing machine was used to generate ultra-thin area with thickness of approximately 100 nm near the center of the small wafers.

The double-jet electro-polishing procedures are described below: (1) prepare three ware glasses with filter paper wet by solutions (two with methanol and one with ethanol) and a beaker of methanol with liquid nitrogen to cool it down; (2) prepare electro-polishing solution (5% perchloric acid (70%) and 95% methanol for 304 SS); (3) pour the solution into the electro-polishing tank and add liquid nitrogen to cool down the solution to approximately -20 ^{o}C; (4) fix the wafer sample on the holder and install it on the electro-polishing machine; (5) obtain the current-voltage curve by auto-test and determine suitable voltage in the flat region; (6) let the double-jet electro-polishing machine do the formal polishing automatically; (7) as soon as the polishing finish, dip the sample to the low temperature methanol in the beaker for 1 minute and then wares for residual solution removal; (8) uninstall the sample from the holder. Note that a successful sample should be shining with small hole/holes near the center.

2.2. Results and discussion

2.2.1. Laser cleaning and Laser shock peening with high energy Nd:YAG laser

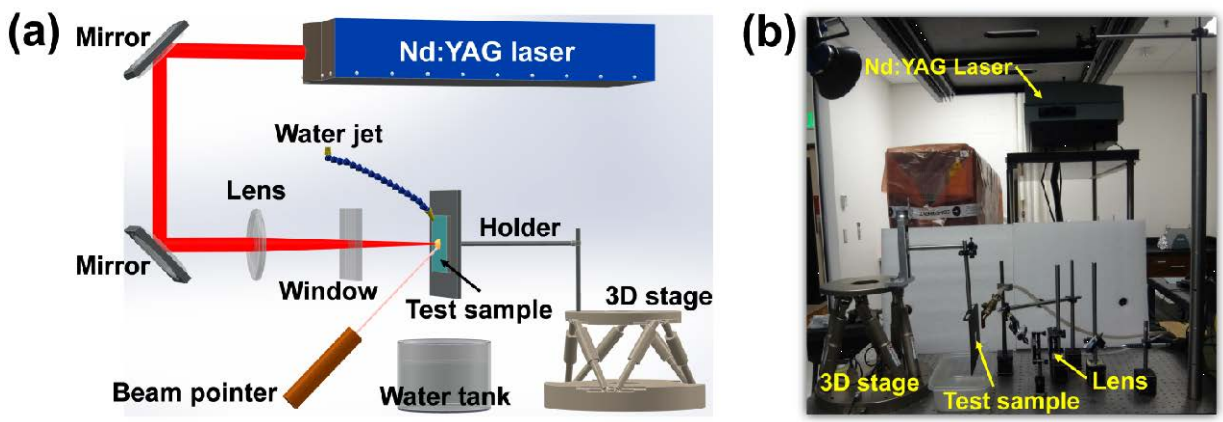

Fig. 2. (a) Schematic diagram of the experimental setup for high energy LSP system. (b) high energy LSP system established in LANE lab.

In this project, in-lab high energy laser shock peening/laser cleaning system was first developed for parameter optimization, material processing, and characterization.

Figure 2a and 2b shows the schematic diagram and practical system of the experimental setup for high energy LSP/laser cleaning system. This system can meet the demands of a single LSP impact and multiple LSP impacts. The laser source is a continuum Q-switched Nd:YAG PR II 8010 laser. The laser pulse frequency could be changed from 1 to 10 Hz. The normally used pulse duration of this laser is approximately 6-8 ns, and the maximum pulse energy is 850 mJ

with a wavelength of 1064 nm. The output diameter of the laser beam from laser is about 5 mm. Two flat Nd:YAG mirrors and a flat convergent lens (focal length: 20 cm) were used to deliver the pulse produced by the laser. The samples were vertically placed at the focal plane. The size of laser spot focused on the samples was measured to be approximately 1~2 mm. In this LSP system, the purified water was used as the confining medium. Control of water purity is important in order to avoid the formation of water bubbles or the concentration of impurities coming from the material ablation due to the laser irradiation. The appearance of suspended elements can affect the LSP process by their interaction with pulsed laser beam. Water in continuous condition is good solution to avoid these elements. Therefore, a special device to produce controlled water jets has been implemented to form a thin water layer on the sample surface to be treated. Taking care of the water velocity and jet direction, it is possible to produce a water layer with constant thickness. Aluminum (Al) foil tape and flat black tape have been chosen as the sacrificial layers. Before LSP experiment, the sample surfaces were covered with an Al foil or a layer of black tape with a thicknesses of ~100 μm. The prepared sample was fixed on a holder and mounted on a motor controlled work stage with resolution of 1 μm and maximum speed of 20 mm/s. The processing parameters of LSP are summarized in Table 2.

Two different LSP experiments were designed. (1) Single spot LSP experiment: we used laser source with a frequency of 1 Hz for conveniently controlling the laser impact times on one point. (2) Large area LSP experiment: we used laser source with a frequency of 10 Hz for large area LSP by adjusting the overlap of laser spots.

Table 2. The processing parameters used in LSP experiment

Laser system	Continuum Nd:YAG PR II 8010 laser; Wavelength: 800 nm; Pulse energy: 850 mJ; Pulse duration: 6-8 ns; Frequency: 1-10 Hz; Beam size: 1~2 mm
Confining medium	Flowing water with layer thickness of approximately 1-2 mm
Sacrificial coating	(1) No coating; (2) Al foil tape (100μm); (2) flat black tape (177 or 100 μm)

2.2.1.1. Laser cleaning with high-energy Nd:YAG laser

In this section, laser cleaning experiments implemented with high energy Nd:YAG laser will be described. Three different kind of contamination layers were used: 1) mixed coatings (mixture of rubber, paint and high temperature resistant coating); 2) black tape; 3) transparent resin.

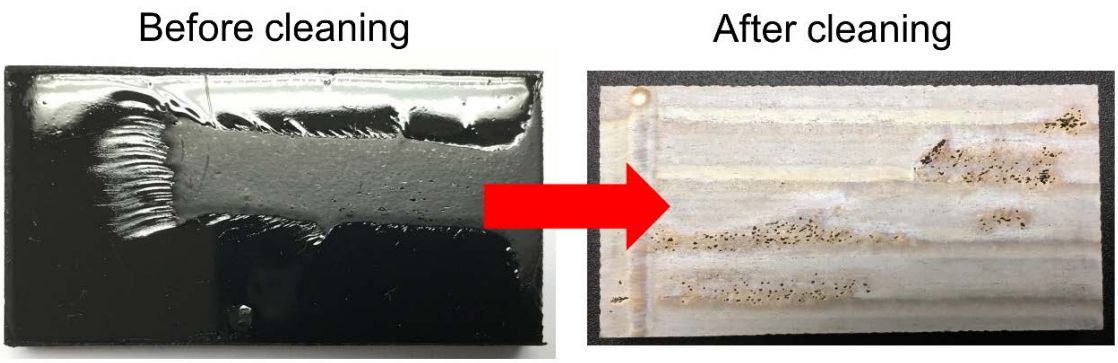

Fig. 3. Laser cleaning of mixed coating. (mixture of rubber, paint and high temperature resistant coating, uneven, 50~100 μm thickness; 850 mJ laser energy, 6~8 ns, 12 mm spot size, 5 mm/s)

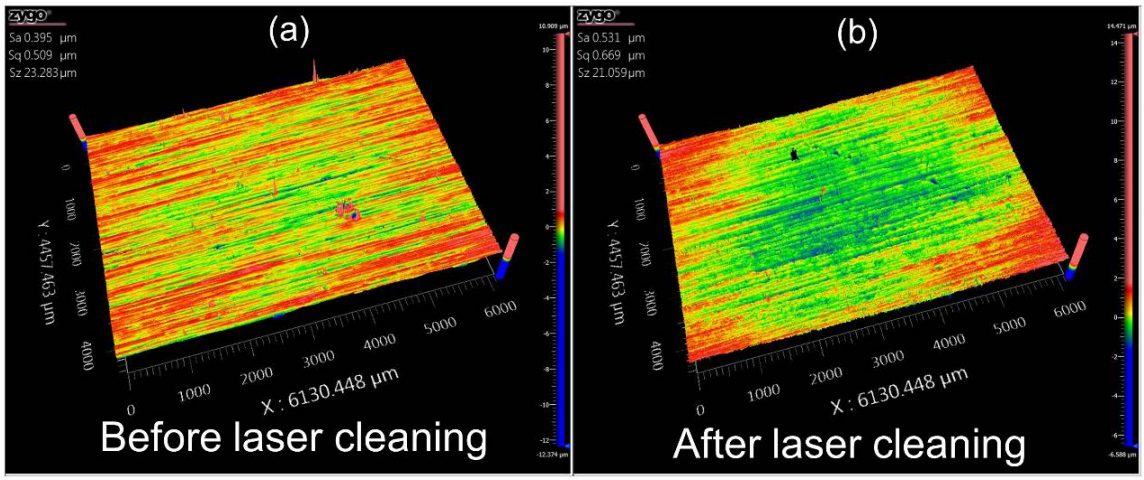

Fig. 4. The Al-Mg alloy surface morphology before/after Nd:YAG laser cleaning (mixed paint)

As shown in Fig. 3., after laser scanning without focusing (850 mJ laser energy, 6~8 ns,12 mm spot size, 5 mm/s) for one time, most of the paint was removed. Some residuals were observed at the places with thick coatings before laser cleaning, which can be removed with the increase of laser scanning times. Surface morphology was measured on the surface before/after laser cleaning (Fig. 4.), showing unchanged or even decreased surface roughness, which indicates the Al alloy surface is not damaged. The decrease of the surface roughness might be caused by the removal of the original surface contamination on the sample surface.

As shown in Fig. 5., after laser scanning with 500 mm focusing lens (850 mJ laser energy, 6~8 ns, 4 mm spot size, 5 mm/s) for one time, the black tape was removed along the scanning line. Some color change was observed after scanning on the sample surface. In addition, the surface morphology after laser cleaning (Fig. 6.) shows increased roughness of approximately 2 μm, indicating slight ablation damage on Al-Mg alloy surface. Although the surface is damaged, the slight roughness increase could be acceptable.

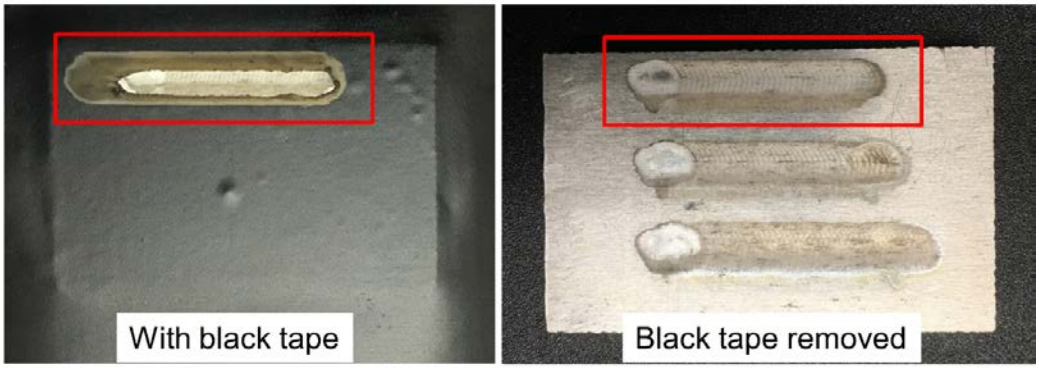

Fig. 5. Laser cleaning of black tape. (100 μm thickness; 850 mJ laser energy, 6~8 ns, 4 mm spot size, 5 mm/s)

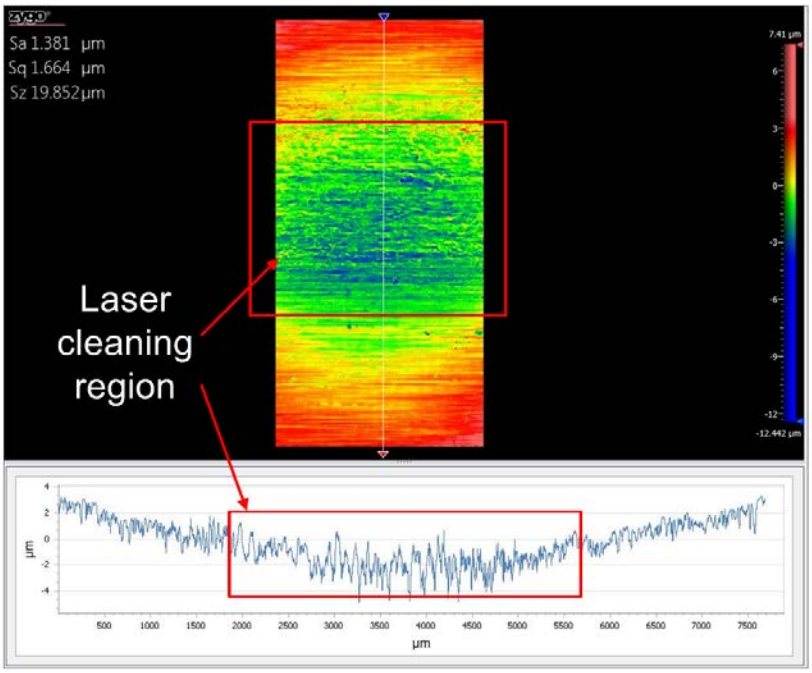

Fig. 6. The Al-Mg alloy surface morphology before/after Nd:YAG laser puissant cleaning (black tape)

As shown in Fig. 7., after laser cleaning with 500 mm focusing lens (850 mJ laser energy, 6~8 ns, 1.5 mm spot size) for one time, the ~2 mm transparent resin was removed completely if the spot-to-spot distance is 2.5 mm (red dashed rectangle). According to the shape of the resin after single point cleaning (yellow dashed rectangle), the cleaning mechanism for the resin removal should be different from that in the previous experiments, which is laser ablation and material burn. Since the resin is transparent, the laser goes through it and ablates the sample surface to generate plasma, which expands rapidly, crushes the resin into pieces and detach it from the sample surface. Shock wave may also play and important role. The surface morphology after laser cleaning (Fig. 8.) shows clear dents and increased roughness of approximately 10 μm, which might be mainly induced by the laser induced shock wave.

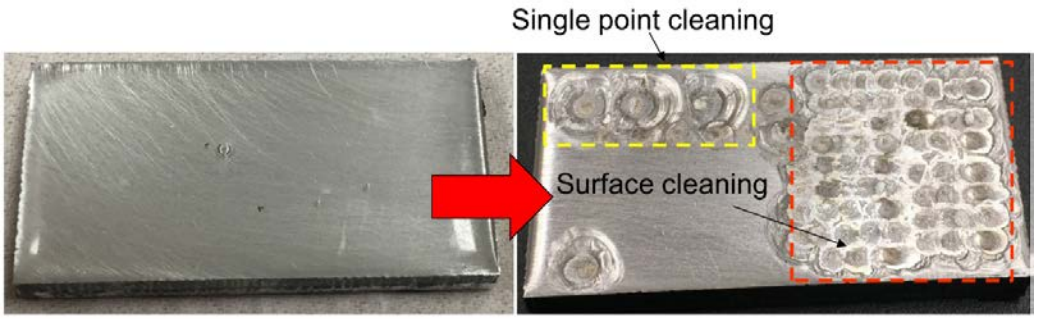

Fig. 7. Laser cleaning of transparent resin. (1-2 mm thickness; 850 mJ laser energy, 6~8 ns, 1.5 mm spot size)

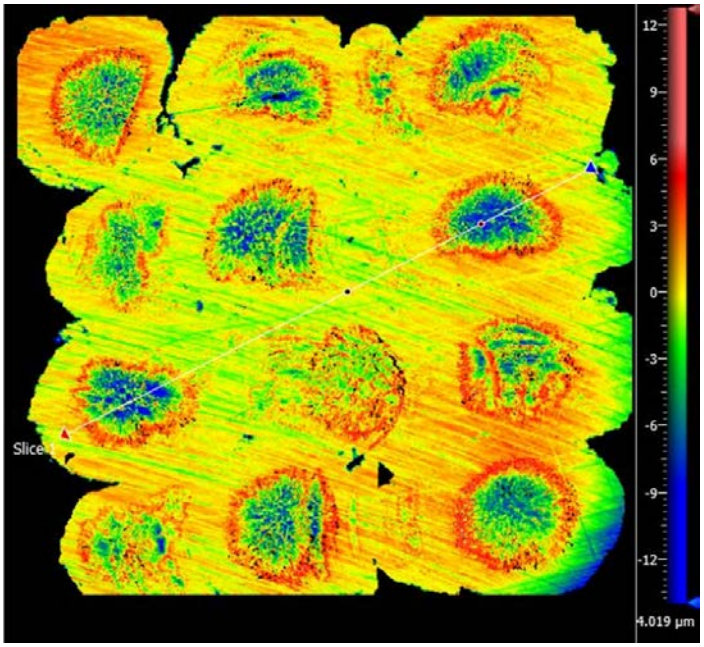

Fig. 8. The Al-Mg alloy surface morphology after Nd:YAG laser cleaning. (transparent resin)

2.2.1.2. Laser shock peening with high energy Nd:YAG laser

LSP with high energy Nd:YAG laser has been researched decades ago and was believed effective for fatigue and corrosion improvements. Therefore, in this project, the first step is to develop a high energy Nd:YAG LSP system, use it for pipeline steel processing, and investigate the pipeline steel property change after LSP.

(a) Parameter optimization with Al-Mg alloy and 304 SS

The important processing parameters related to LSP conditions are laser processing parameters, confining medium, and sacrificial coatings, which can significantly affect the mechanical/ fatigue/corrosion properties of the alloy and metallic materials. Therefore, the objective of this section is to investigate and optimize the effect of these key factors on LSP using Al-Mg alloy and 304 SS as the test samples, which can reflect LSP effect obviously.

Sacrificial coating effects

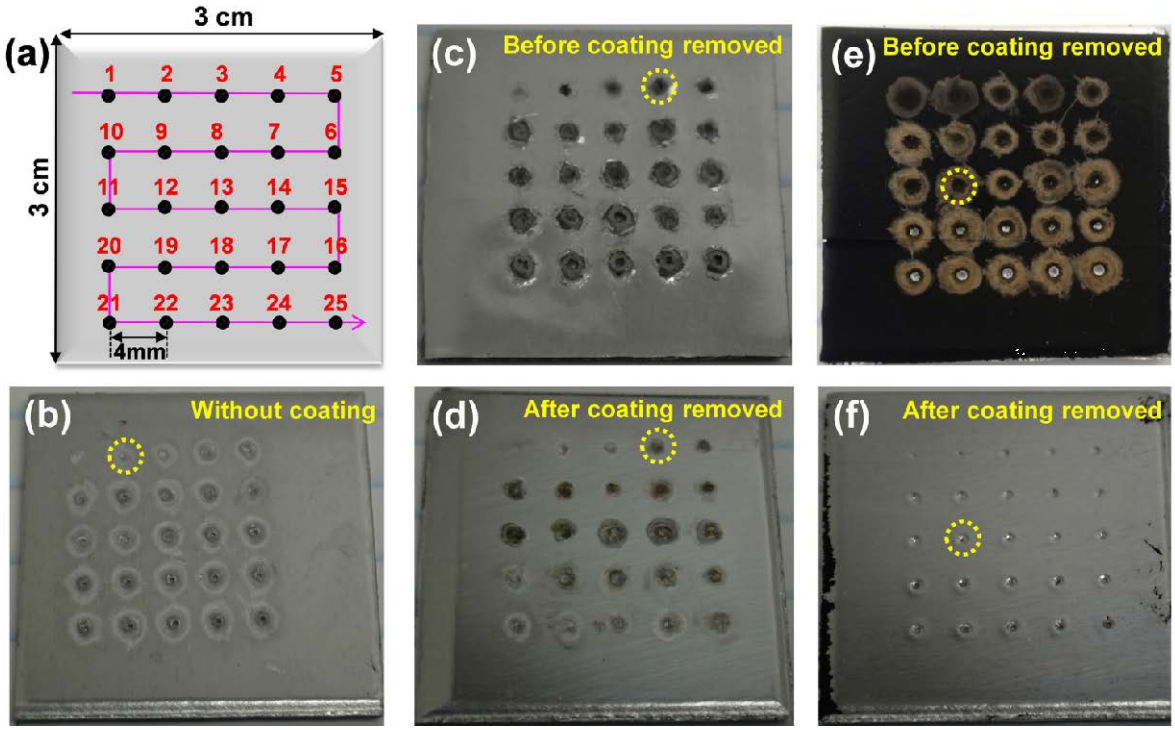

Fig. 9. (a) Schematic of the point distribution with different LSP impacts. (b-f) Laser-peened Al-Mg alloy samples (b) without sacrificial coating, using (c,d) Al foil tape and (e,f) black tape as the sacrificial coatings.

The use of absorbent sacrificial coatings is found to increase the shock wave intensity in addition to the protection of the sample's surface from laser ablation and melting. Therefore, it is very important to select the effective and practical sacrificial coatings for LSP applications. In Fig 9a, the schematic of LSP-impacted points on Al-Mg alloy samples with different impact times from 1 to 25 is shown. The distance between nearby impacted points is about 4 mm, which could avoid the interactions among different points. Figures 9b to 9f show the optical images of laser-peened Al-Mg alloy sample plate (b) without sacrificial coating, using (c,d) Al foil tape, and black tape as the sacrificial coatings, respectively. Obviously, increasing LSP impact times could result in higher possibility of laser damage to the sample surfaces. The dashed yellow circles used in Figs. 9b to 9f indicate the impacted points from which the penetration of the sacrificial coating or alloy surface damage could be observed. In Fig. 9b, laser-peened sample plate without any sacrificial coating shows surface damage from 2 LSP impacts. Figures 9c and 9d show the laser-peened sample with Al foil as sacrificial coating (c) before and (d) after coating removed, respectively. The penetration of the coating in Fig. 9c and the damage of alloy surface in Fig. 9d both begin from 4 LSP impacts. The laser-peened samples with black tape as sacrificial coating before and after coating removed are shown in Fig 9e and 9f, respectively. However, under this

condition, the penetration of coating and the damage of alloy surface start from 12 LSP impacts, which is much higher than that with Al foil. Apparently, the black tape could endure more laser impacts than Al foil, while it is easier for the LSP without sacrificial coating to damage the sample surfaces. The surface damage induced by laser direct irradiation should be avoided during the LSP process, which could increase the surface roughness, decrease the residual stress and reduce the corrosion resistance. On the other hand, higher impact times are preferred to generate higher residual stress and better corrosion resistance. Thus, the black tape is considered to be the prior sacrificial material and will be used in the following experiments.

Laser pulse energy and spot size effects

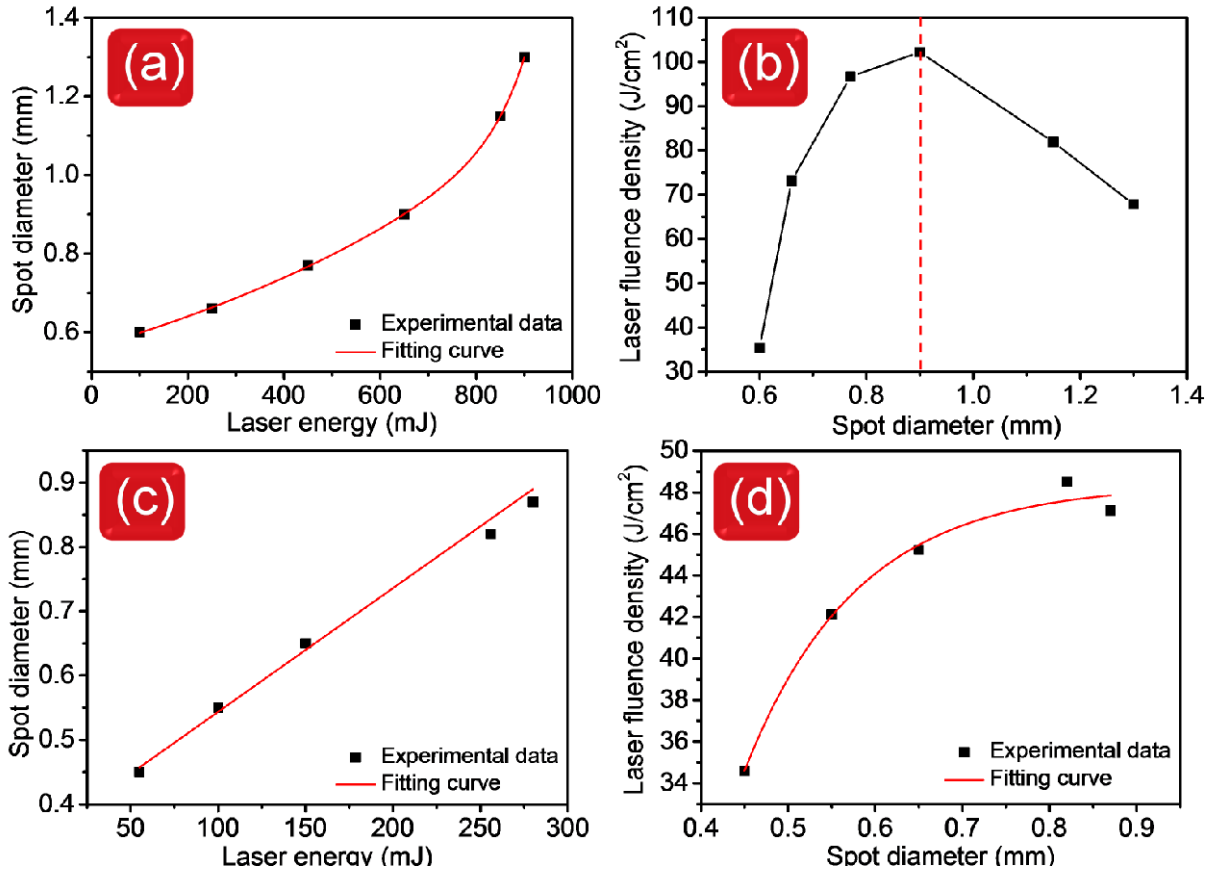

Fig. 10. Dependence of (a) spot diameter on laser energy and (b) laser fluence on spot diameter with 1064 nm wavelength; dependence of (c) spot diameter on laser energy and (d) laser fluence on spot diameter with 532 nm wavelength.

Figure 10 shows the relationship between laser pulse energy/fluence density and the spot size under two different wavelengths of 1064 nm (10a, 10b) and 532 nm (10c, 10d). At the wavelength of 1064 nm, laser spot diameter increases exponentially from 0.6 to 1.3 mm with laser pulse energy increasing from 100 to 900 mJ (Fig. 10a), from which a peak laser fluence density of approximately 102 J/cm^2 is obtained at moderate laser output energy of 650 mJ and

corresponding spot diameter of 0.9 mm (Fig. 10b). On the other hand, at the wavelength of 532 nm, a linear relationship between spot diameter and laser pulse energy were observed, as is shown in Fig. 10c, leading to peak power density of approximately 48 J/cm^2 at nearly the highest pulse energy and spot size (Fig. 10d). The relationship between spot diameter and laser energy for wavelengths of 1064 nm and 532 nm is different, which should be attributed to limited pulse energy at 532 nm (less than 300 mJ). In fact, for pulse energy less than 650 mJ (with peak fluence density) at 1064 nm, the spot size also increases linearly with laser energy.

After confirming the relationship between laser pulse energy and spot size, different laser pulse energies from 100 to 850 mJ were used for laser shock peening on Al-Mg alloy surface. Figure 11 compares the 3D morphologies (a-e) and optical images (f-j) of the Al-Mg alloy surfaces treated by single pulse LSP with laser energy of (a, f) 100, (b, g) 250 (c, h) 450, (d, i) 650, and (e, j) 850 mJ. The cross section profile of the dent along the lines in Fig 11a-11e is shown in Fig. 11k, demonstrating the obvious increase in both dent depth and dent diameter with the increment of laser pulse energy. Specifically, the dent diameter as a function of laser pulse energy are shown in Fig. 11I, the dent diameter is increased rapidly with the increment of laser energy, which is the similar to the relationship between spot diameter and laser pulse energy (Fig. 10a).

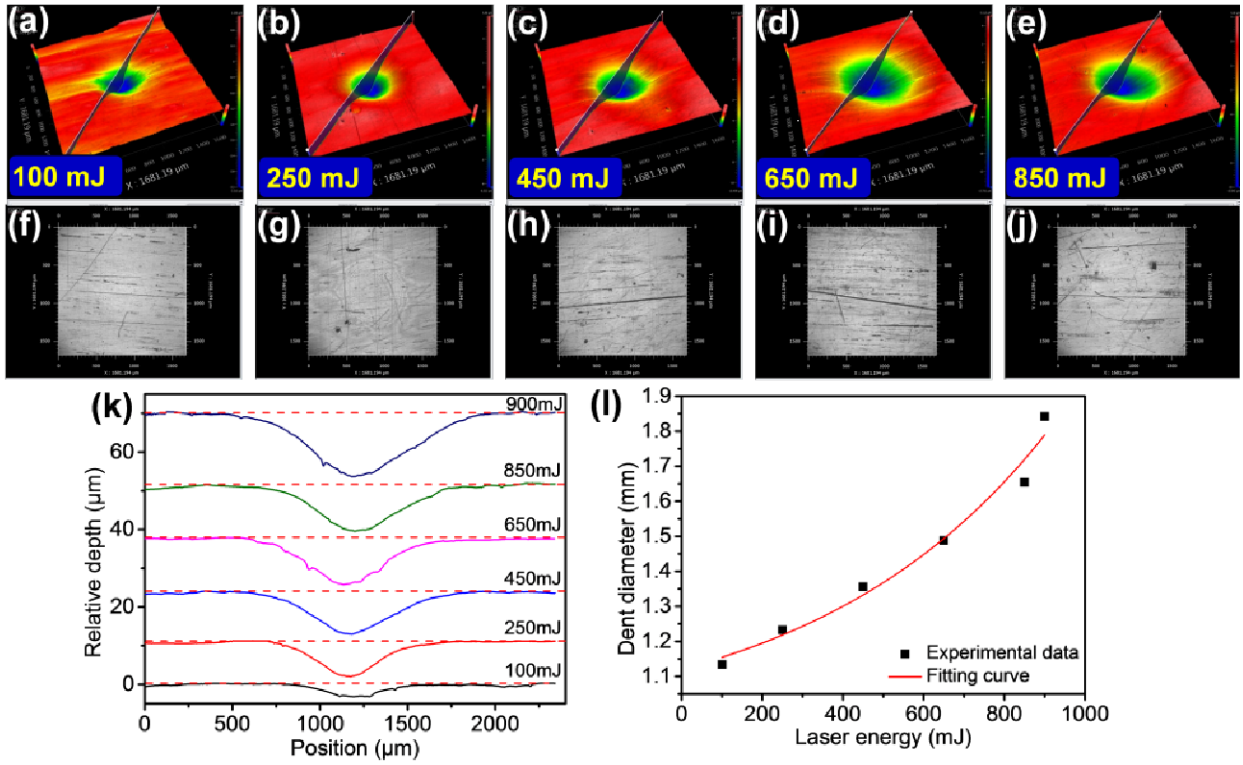

Fig. 11. (a-e) 3D surface topographies of the Al-Mg alloy surfaces treated by single pulse LSP with laser energy of (a) 100, (b) 250 (c) 450, (d) 650, and (e) 850 mJ. (f-i) Corresponding optical images of the Al-Mg alloy shown in (a-e). (k) Dent depths with different laser energy. (l) The dent diameter as a function of laser energy.

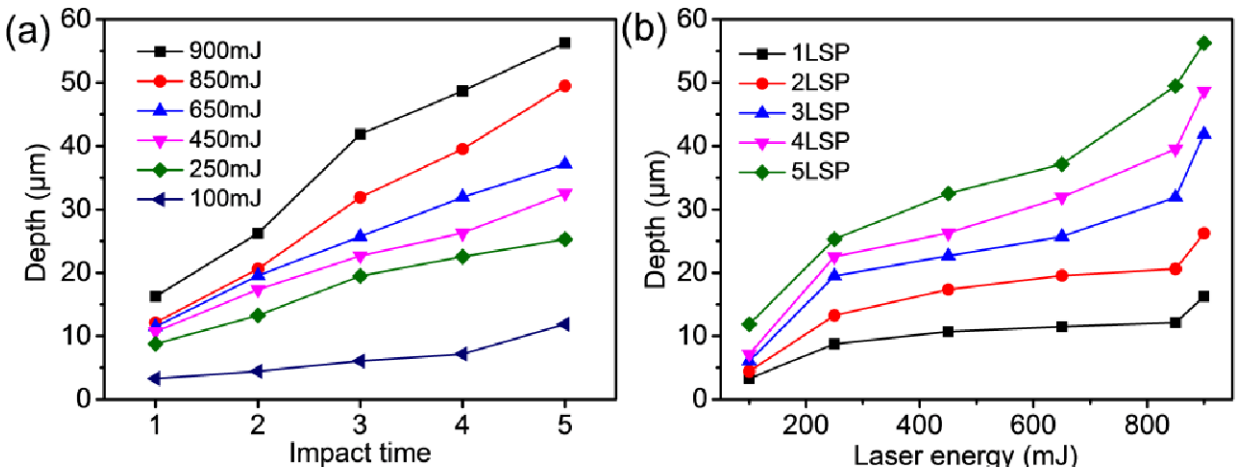

Fig. 12. The depth of dent center as a function of (a) impact time and (b) laser energy.

Figure 12 shows the center depth of the dent on Al alloy surface as a function of (a) impact time and (b) laser energy. It can be seen from Fig. 12a that all the curves for different laser pulse energy are nearly linear while with different slopes. The higher the pulse energy, the bigger the slope is, indicating more effective LSP effect with higher laser energy. Figure 12b plots the dent depth versus laser pulse energy. Two critical pulse energies could be point out. First, at 100 mJ pulse energy, the dent depth increases very slowly and only LSP with 5 impacts could the dent depth be larger than 10 μm, indicating a serious loss in shock wave pressure and the approach to the limit energy of plasma and shock wave generation. Second, a steep increase could be observed from 850 mJ to 900 mJ, which might need further research by LIBS and pressure measurement. Overall, the depth at the dent center increases with the increment of both LSP impact times and laser pulse energy. It should point out that, although the laser power density decreases from 102 Jw/cm^2 to 68 J/cm^2 with pulse energy increasing from 650 mJ to 900 mJ (Fig. 10b), the dent depth remains increasing at all impact times (Fig. 12b), indicating that both the laser fluence and the spot size contributes to the pressure value of the laser induced shock wave.

Laser wavelength effects

Laser wavelength is another processing parameter which could affect the shock wave pressure. Therefore, some experiments were conducted with two different wavelength of the Nd:YAG laser. As shown in Fig. 13a and 13b, the dent depth versus laser pulse energy are plotted under different wavelengths (1064 nm, 532 nm) for 1 impact and 5 impacts, respectively. Compared with the shorter wavelength (532nm), longer wavelength (1064nm) is found to be slightly more efficient for the LSP effect. It is believed that the laser wavelength affects the shock wave in three aspects: 1) absorption coefficient of the water overlay; 2) laser and metal interaction efficiency; 3) dielectric breakdown threshold of the transmitting medium. In our experiment, although 532 nm has lower absorption coefficient in water and higher photon-metal interaction

rate compared to 1064 nm, its low dielectric breakdown threshold could result in much more energy cost in laser transmission, and thus limit the shock wave pressure to a value lower than the shock wave generated by 1064 nm laser pulse with the same energy.

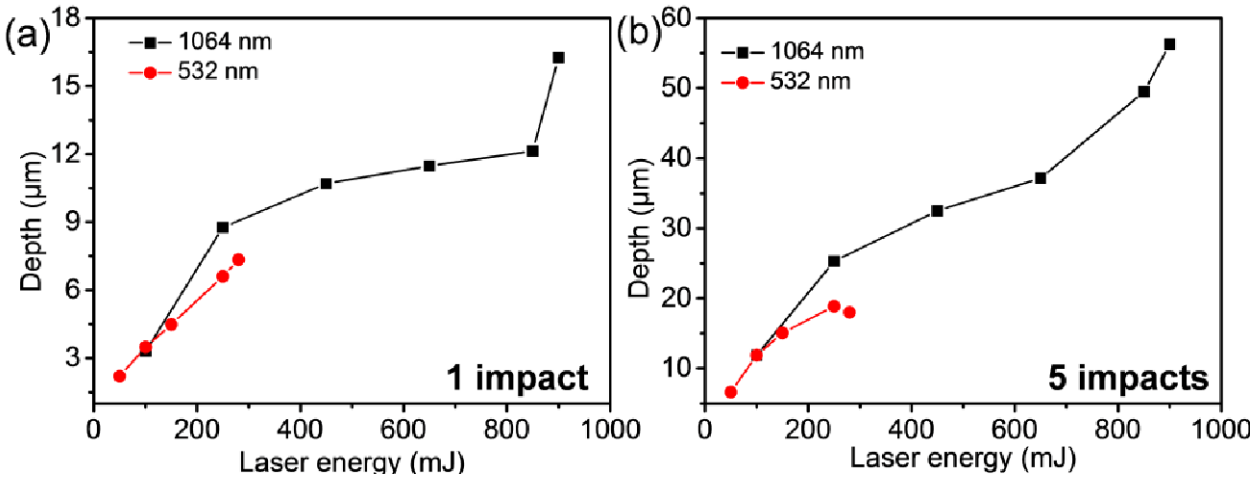

Fig. 13. The depth of dent center vs laser energy with laser wavelengths of 1064 and 532 nm for (a) 1, and (b) 5 impacts.

Effects of the surface structure of the sacrificial coating

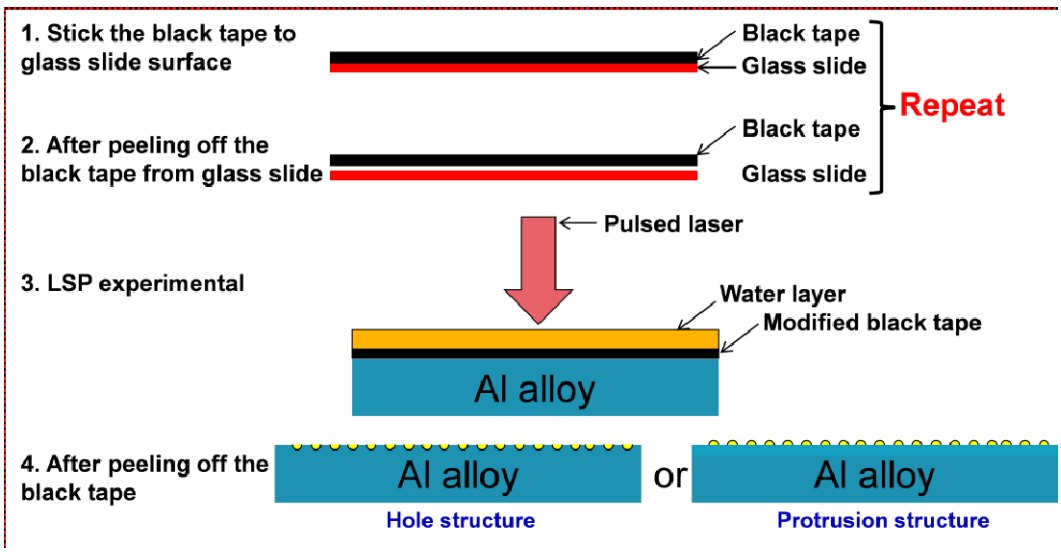

Fig. 14. Schematics of the laser shock induced hole/protrusion formation process.

In our LSP experiments, it was recognized that the black tape conditions could result in different structures on the sample surface, such as holes or protrusions. Thus, a procedure in Fig. 14 was designed to quantitatively model different black tape conditions. By sticking the black tape to glass slide surface and then peeling off, the change of the black tape surface was achieved. Next, the same treatment was repeated for different times and the modified black tape was attached onto the Al-Mg alloy surface to finish the sample preparation with different black tape conditions.

After the LSP experiments, the sample surface structures were examined by Zygo 3D profile meter and optical images.

For reference, black tape without any treatment was used for LSP treatment with different impact times. Figure 15 shows the (a-e) 3D surface morphology and (f-j) optical images of the Al-Mg alloy after single spot LSP for 1-5 impact times. No obvious localized surface roughness is observed and few micro holes/protrudes are found. The similar results are also observed on the surfaces of 304 SS and CS (not shown here). The dent depth as a function of LSP impact times are plotted for Al-Mg alloy (Fig. 15k), 304 SS (Fig. 15l), and CS (Fig. 15m), where the dent depth changes from 20 to 80 μm for Al-Mg alloy, 4 to 11 μm for 304 SS, and 2 to 8 μm for CS. A linear relationship between the dent depth and LSP impact times is observed for different materials, but the slopes vary: Al-Mg alloy > 304 SS > CS.

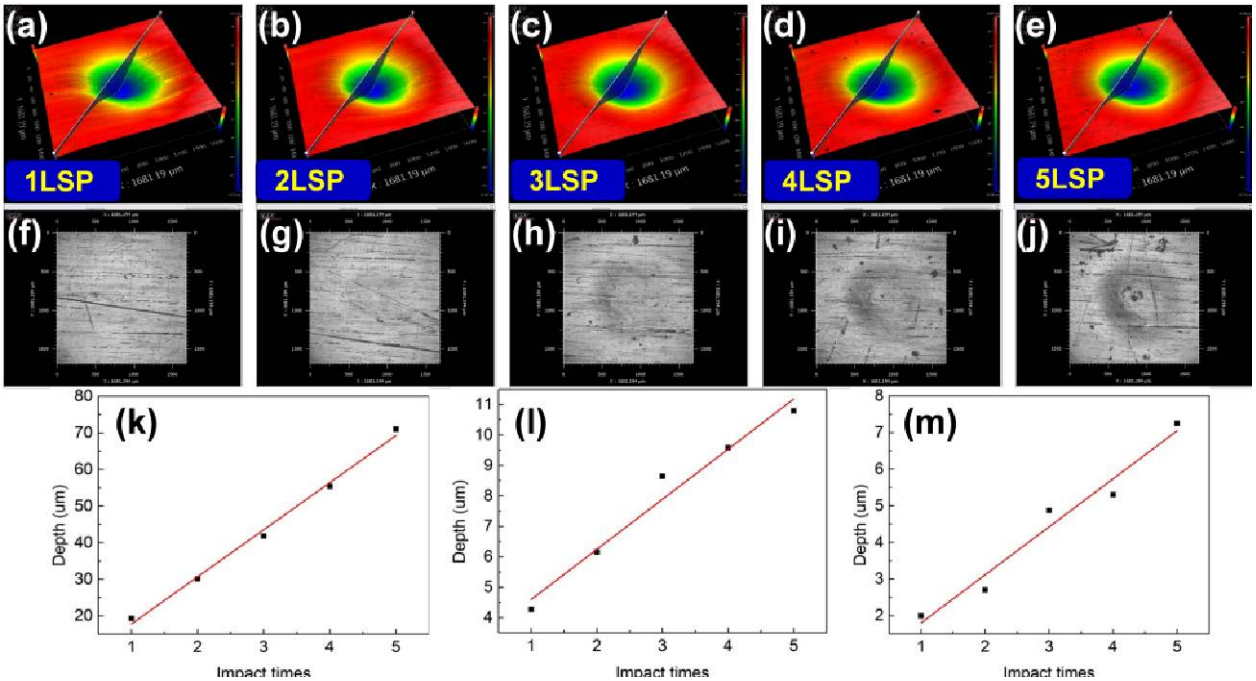

Fig. 15. (a-e) 3D surface topographies of the Al-Mg alloy surfaces treated by single pulse LSP for (a) 1, (b) 2, (c) 3, (d) 4, and (e) 5 impacts. (f-j) Corresponding optical images of the Al-Mg alloy shown in (a-e). Dependence of dent depth on pulsed laser impact time for (k) Al-Mg alloy, (l) 304 SS, and CS.

Fig. 16 shows 3D surface topographies and optical images of the Al-Mg alloy surfaces treated by single pulse LSP with black tape sticking to/peeling off from glass slide for (a, e) 0, (b, f) 1, (c, g) 2, and (d, h) 5 times. Uniform micro holes/protrudes were formed by LSP with modified black tapes. It could be observed that with increasing of the modification times, the micro holes/protrudes become more intensively distributed, and the holes/protrudes sizes become larger.

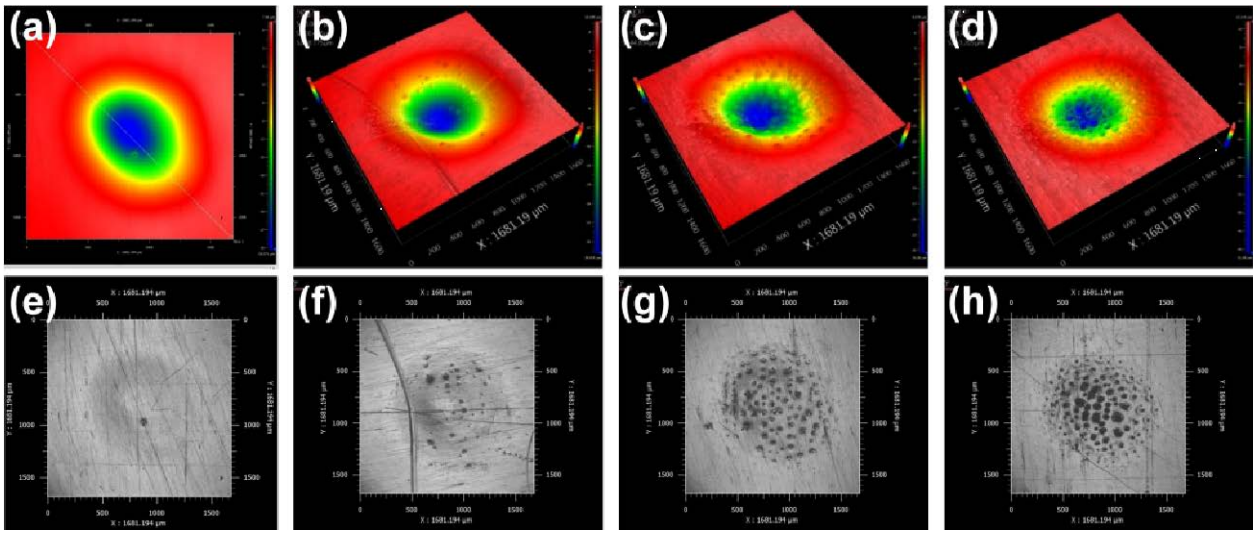

Fig. 16. (a-d) 3D surface topographies of the Al-Mg alloy surfaces treated by single pulse LSP with black tape sticking to/peeling off from glass slide for (a) 0, (b) 1, (c) 2, and (d) 5 times. (e-h) Corresponding optical images of the Al-Mg alloy shown in (a-d).

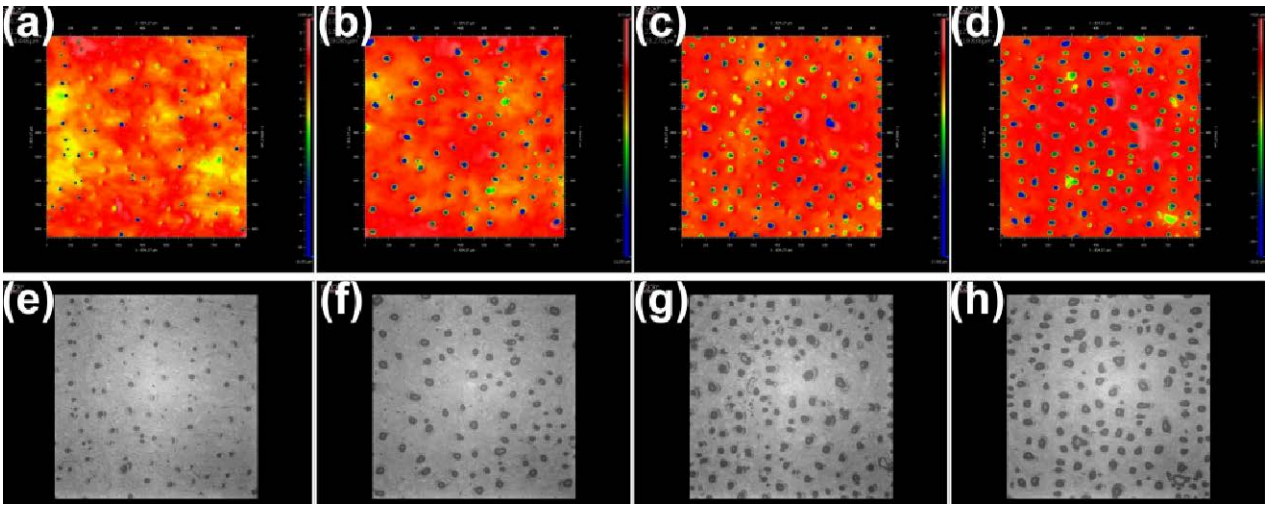

Fig. 17. (a-d) 3D surface topographies of the black tape surfaces (a) without treatment, (b) after sticking to/peeling off from glass slide for (b) 1, (c) 2, and (d) 5 times. (e-h) Corresponding optical images of the black tape shown in (a-d).

In Fig. 17, the surface morphology and optical images of the black tape surface without treatment (Fig. 17a, e), with treatment for 1 time (b, f), 2 times (c, g), and 5 times (d, h) indicate that the small holes on the tape surface obviously increase from ~25 μm (0 time) to ~35 μm (1 time), ~40 μm (2 times), and ~50 μm (5 times). The small holes on the black tape surface changes from small and sparse to large and dense as the increasing of the treatment times. It is assumed that the micro holes/protrudes formed on Al-Mg alloy sample surface were induced by the holes on the black tape surface. There should be a threshold for the hole diameter on the

black tape surface for the micro dents/protrudes generation on sample surface.

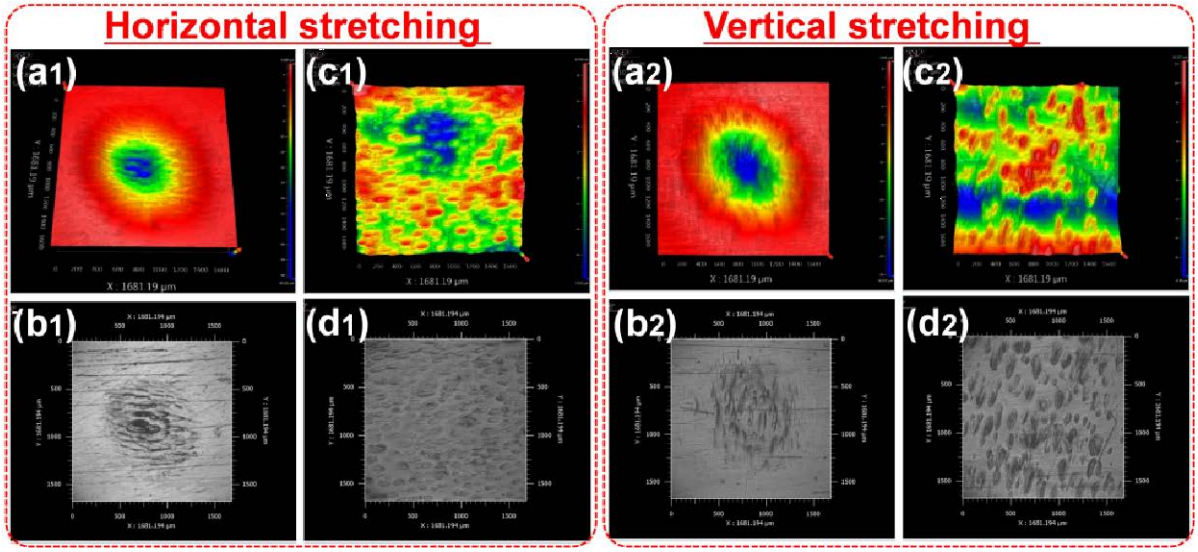

Fig. 18. (a_1-d_1) 3D surface topographies of the Al-Mg alloy surfaces treated by (a_1, b_1) single pulse and (c_1, d_1) large area LSP after black tape horizontal stretching treatment. (a_2-d_2) 3D surface topographies of the Al-Mg alloy surfaces treated by (a_2, b_2) single pulse and (c_2, d_2) large area LSP after black tape vertical stretching treatment.

To confirm the relationship between the tape surface structure and the generated micro holes/protrusions on sample surface, another tape surface modification method is applied. The black tape was stretched horizontally/vertically and attached to the Al-Mg alloy surface without release. As shown in Fig. 18, with horizontally stretched black tape as sacrificial layer, the sample surface after both single spot LSP and large area LSP show long and narrow micro holes/protrudes along the horizontal direction. For single spot LSP, protrudes distributed around and inside the dent except for the center of it (Fig. 18a_1, b_1). For large area LSP, protrudes distributed extensively and holes are scarce (Fig. 18c_1, d_1). With vertically stretched black tape attached to the Al-Mg alloy without release, long and narrow holes/protrudes along the vertical direction are observed. The same distribution phenomena of holes/protrudes in single spot LSP and large area LSP applied as the samples with horizontally stretched black tape, except for the direction (Fig. 18a_2-d_2).

Figure 19 shows the surface morphologies and optical images of black tape without processing (a,f), after stretching horizontally for 120% (b,f), 140% (c, h), and combination of sticking to/peeling off from glass slide for 5 times and horizontally stretching for 120% (d, i) and 140% (e, j). No obvious change for hole diameter is observed only by stretching, while the elongation could be easily observed by combining sticking/peeling and stretching. The 140% stretching leads to larger elongation than that of 120% stretching. The formed spindle holes/protrudes microstructures on the laser-peened metal surfaces are believed to have a direct relationship with

the small hole elongation on the black tape surface.

In general, the size, shape, and density of the micro holes/protrudes microstructures could be effectively controlled by surface treatment of the black tape before LSP. A close relationship exists between the hole size/structure on the applied black tape and the generated micro holes/ protrudes microstructures on the sample surfaces. It is known that the defects on the metal surface might become the initiation points of corrosion. The research results obtained in this part will help to avoid undesired micro dents/protrudes defects forming on the laser-peened metal surface by carefully controlling the tape and sample preparation process.

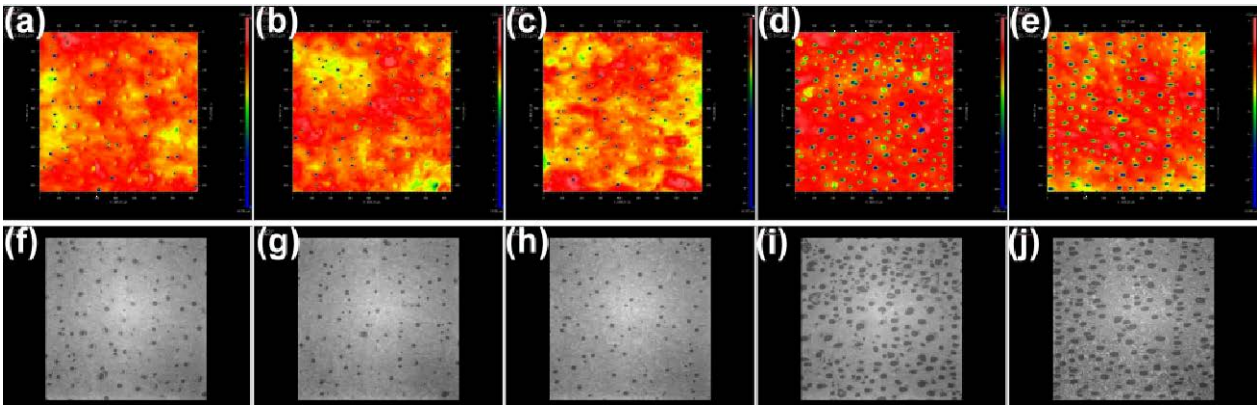

Fig. 19. (a-e) 3D surface topographies of the black tape surfaces (a) without treatment, after stretching with stretch ratio of (b) 120% and (c) 140%, and after sticking to/peeling off from glass slide for 5 times and then stretching with stretch ratio of (d) 120% and (e) 140%. (f-j) Corresponding optical images of the black tape shown in (a-e).

Laser shock bending phenomena induced by large area LSP

Laser shock bending is of significant value to aerospace, automotive, ship building and micro electronics industries. Conventionally, the laser bending process is achieved by introducing thermal stress into the work-piece by irradiation with a focused laser beam. Recently, non-thermal bending using a high energy pulsed laser has generated growing interest. Similar to the laser shock peening process, high-pressure and compressive shock wave are induced onto the target material by high-energy laser pulses. This non-thermal, shock-wave bending mechanism is often denoted as laser shock bending.

In our lab, laser shock bending phenomenon has been observed during the large area LSP processing of Al-Mg alloy plates with thickness of approximately 2 mm, as is shown in Fig. 20. The sample bending direction is perpendicular to the laser scanning direction. It is clear that the deformation mechanism of this Al-Mg alloy is positive under the laser energy of 800 mJ. The bending angle (Fig. 20d) increases linearly with the LSP impact times, changing from 0° before LSP, to 6°, 11°, and 16° after 1, 2 and 3 times of large area LSP, respectively. It is considered

that the deeper compressive stress achieved by LSP leads to the formation of tighter curvatures.

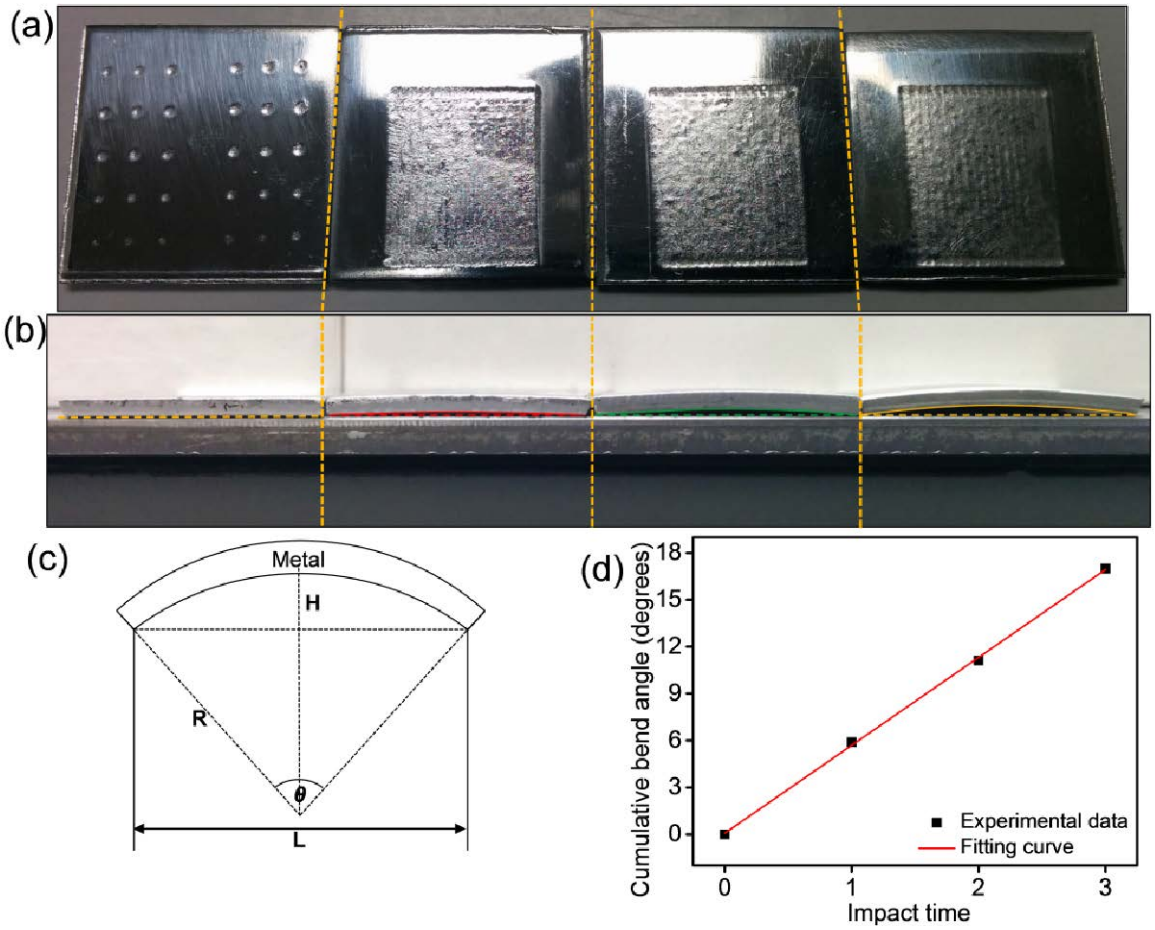

Fig. 20. A large area laser shock peening formed Al-Mg alloy with different impact time. (a) Top view, (b) side view. (c) The model for calculating the laser shock bend angle, (d) dependence of bend angle of Al-Mg alloy on pulsed laser impact times.

Further parameter optimization using 304 SS

304 stainless steel (SS) is one of the most popular pipeline materials due to its high strength and high corrosion resistance. For single point LSP experiment, the influence of LSP impact times on surface roughness and morphology of the 304 SS sample plate was investigated and is shown in Fig. 21. It is observed from the SEM images (Fig. 21a-e) that the small dents and defects increase generally as LSP impacts arise from 1 to 10, indicating the increase of the localized surface roughness. Figures 21f-j exhibit the corresponding 3D surface profiles of the dents with 1, 2, 4, 7, and 10 LSP impacts, and the cross-sectional profile is shown in Fig. 21k. The dent depth is observed to increase with the LSP impact times. Figure 21l shows the depth of dent center as a function of LSP impacts. The depth of the dent center increases nearly proportionally to the LSP impact times and a linear fitting curve could be made with acceptable standard deviation.

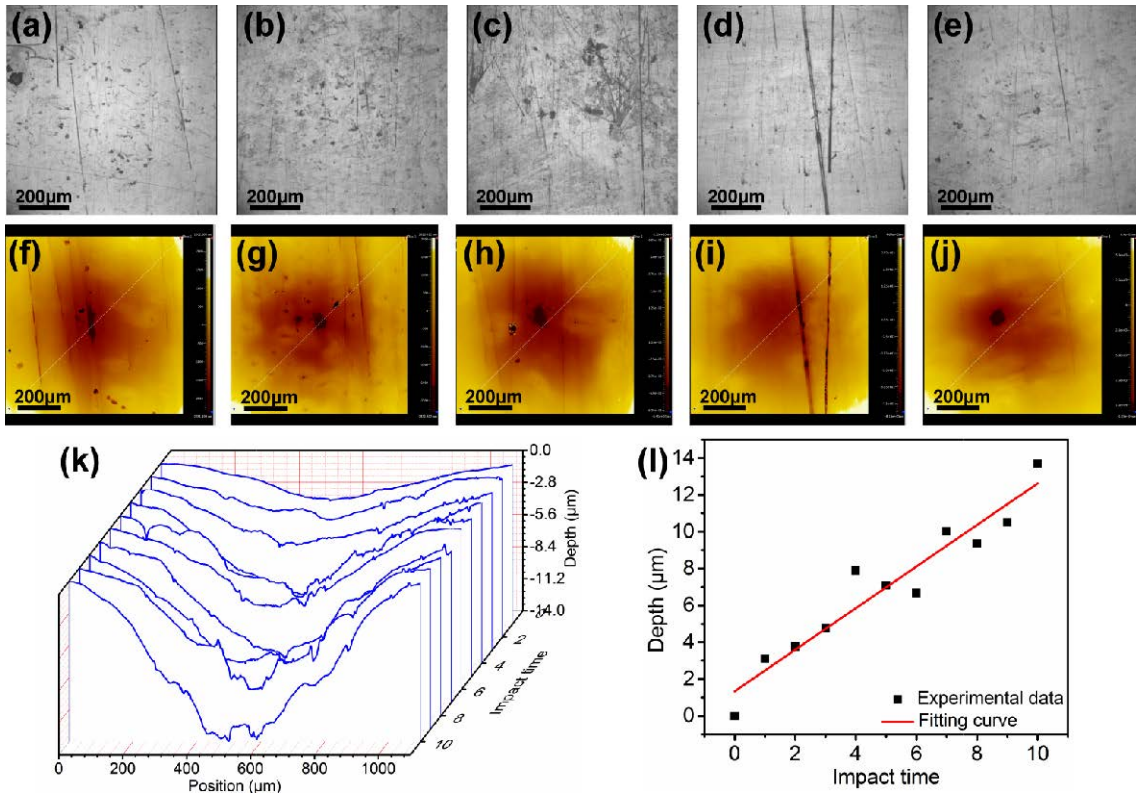

Fig. 21. (a-e) SEM images and (f-j) corresponding 3D surface topographies of the 304 SS sample surfaces by single pulse laser shock peening for (a) 1, (b) 2, (c) 4, (d) 7, and (e) 10 impacts. (k) Dent depths with different laser pulse impacts. (l) The depth of dent center as a function of LSP impacts.

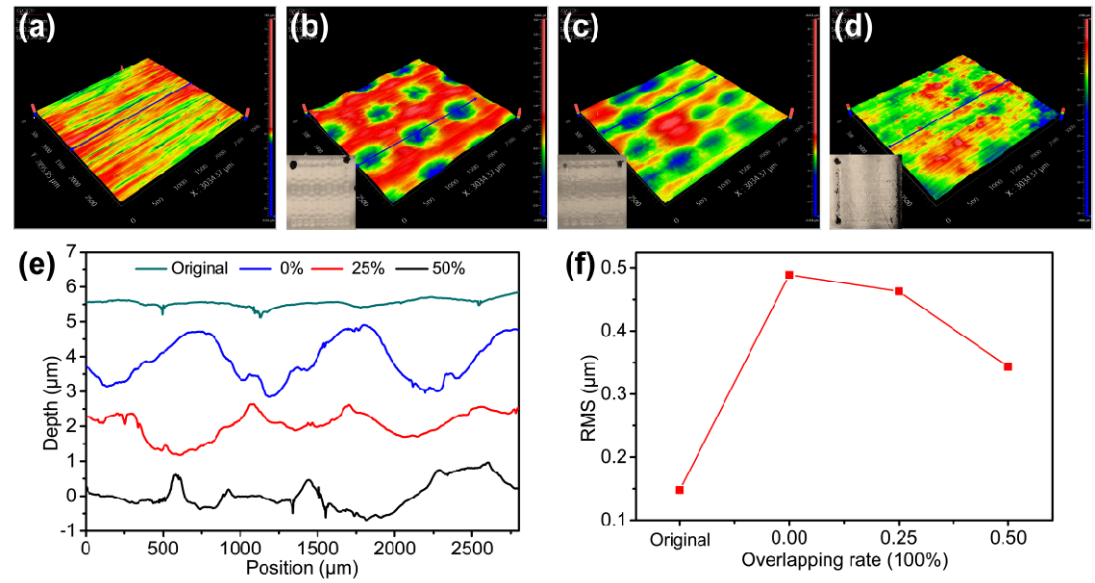

Fig. 22. 3D surface topographies of the 304 SS sample surfaces (a) before LSP and (b-d) after LSP with different overlapping rates of (b) 0%, (c) 25%, and (d) 50%. Insets in (b-d) show the corresponding optical images of the samples in the same images. (e) Surface deformation of the same sample along the line in the corresponding images. (f) Comparison of surface roughness with different overlapping rates.

Large area LSP experiments were also implemented on 304 SS with different overlapping rates. As shown in Fig. 22, LSP with different overlapping rates were carried out and corresponding 3D topographical images as well as the optical photos (a-d) are provided. Fig. 22a show the sample surface without any LSP process, which is the most flat, followed with the samples after LSP (Figs. 22b-d) with 0%, 25%, and 50% overlapping rates, respectively. LSP with 75% overlap will seriously damage the sample surface and thus ignored. As we can see, the LSP induced dents become smaller when the overlapping rate increases from 0% to 25%, which is due to the decrease of distance between LSP points. Different from 0% (Fig. 22b) and 25% (Fig 22c), with overlapping rate of 50% (Fig 22d), no regular or obvious dent patterns could be found on the relatively flat surface. The cross-sectional view of the dents with overlapping rates (Fig. 22e) show the abrupt dent generation from original sample to laser-peened sample with 0% overlap, as well as the gradually flattened surface with the overlapping rate increasing from 0% to 50%. Though some small protrude points is observed in Fig 22d, similar with the phenomenon on the laser-peened Al-Mg alloy samples, the surface roughness still decrease as overlapping rates increase from 0% to 50%, as is shown in Fig. 22f. In conclusion, 50% overlap is the most favorable for large area LSP on 304 SS.

<u>(b) Mechanical property improvement after LSP</u>

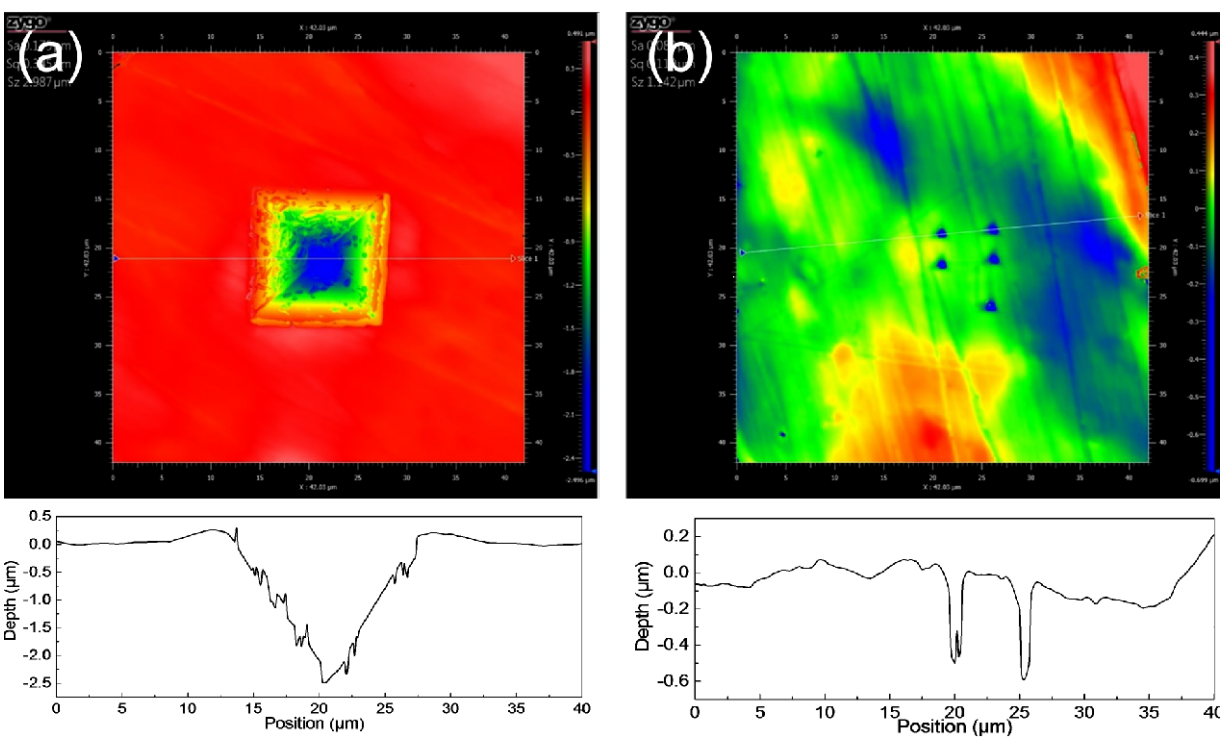

Fig. 23. 3D surface morphologies of Al alloy after (a) micro-hardness test and (b) nano-indentation test. Inserts in (a) and (b) show the cross-sectional height profiles along the lines in the corresponding images.

In this section, hardness measurements and analyses were carried out on single spot and large area LSP samples using two different methods: Vickers micro-hardness test and nano-indentation. Figure 23 compares the 3D surface profiles of Al alloy surfaces after (a) Vickers micro-hardness test and (b) nano-indentation test. It can be observed that Vickers hardness affects a square area with a side length of 30 μm and a depth of 2.5 μm, while nano-indentation affects a triangle area with a side length of ~ 2 μm and a depth of 0.5 μm. Since the LSP-affected area and depth are nearly 1 mm diameter and 1 mm depth, respectively, both nano-indentation and Vickers micro-hardness test can be used for localized hardness measurement.

Average surface nano-indentation tests after single-spot LSP

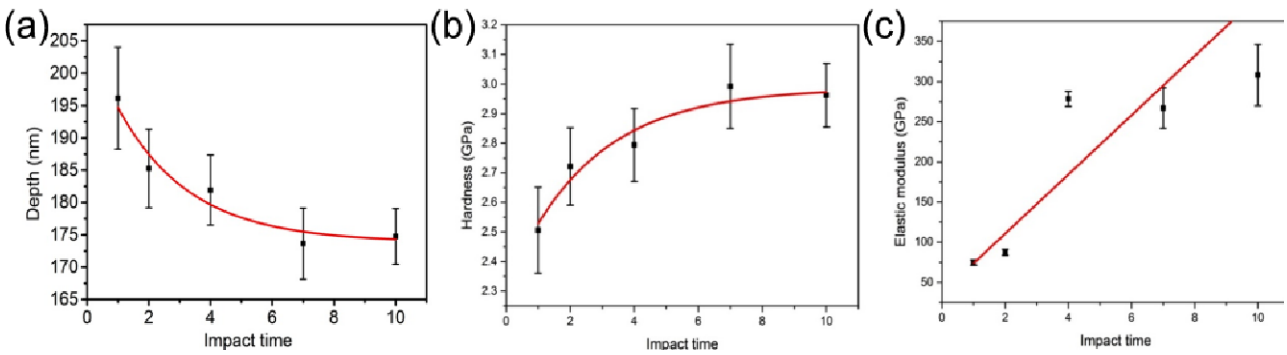

Fig. 24. The profiles of the (a) contact depth, (b) surface nano-hardness, and (c) elastic modulus on 304 SS sample surfaces as a function of LSP impact times.

The surface nano-indentation results for 304 stainless steel samples after LSP are presented in Fig. 24. Figure 24a shows the dependence of contact depth on LSP impact times. With the increase of LSP impacts, the contact depth decreases and tends to become stable. Figure 24b and 24c exhibit the dependences of the surface nano-hardness and elastic modulus of the 304 SS samples on LSP impact time. The values of the surface nano-hardness and elastic modulus for the laser-peened 304 SS are obviously larger than those of non-laser-peened samples. In addition, the values of surface nano-hardness and elastic modulus of the sample increase with the increment of the LSP impact times. With maximum of 10 LSP impacts, the nano-hardness and elastic modulus are increased by 18.4% and 313%, respectively, compared with that of the non-laser-peened region. The improved the nano-hardness and elastic modulus are considered to be favorable in enhancing the stiffness and the possible corrosion resistance of the stainless steel.

Average surface microhardness tests after single-spot LSP

The Vickers micro-hardness tests were carried out on three kinds of laser-peened materials, including Al-Mg alloy, 304 SS, and CS. As shown in Fig. 25a-c, to realize precise measurement of Vickers micro-hardness, the load curve dependences of hardness are firstly measured on none laser-peened areas for (a) Al-Mg alloy, (b) 304 SS, and (c) CS. The standard is that the loads at

the flat area of the curve where the hardness does not change with different loads are suggested for normal test. For our conditions, the load of 0.05 kg is selected for all samples, where the hardness value is close to normal one, while the load could also enable easy multiple tests in the small test areas.

Figures 25d-e show the Vickers micro-hardness as a function of LSP impacts for (d) Al-Mg alloy, (e) 304 SS, and (f) CS, respectively. The values of the surface micro-hardness for the laser-peened Al-Mg alloy and 304 SS samples are both obviously larger than those of samples without LSP. In addition, the surface micro-hardness of the sample increases with the increment of the LSP impacts. With maximum of 5 LSP impacts, the micro-harnesses of laser-peened Al-Mg alloy and 304 SS are increased by 20.6% and 39.3%, respectively. The micro-hardness measurement results are similar to nano-indentation measurement results, confirming that the surface hardness is improved by LSP and increased with the increment of the LSP impacts. For CS, the Vickers micro-hardness does not increase obviously and even decreases with 4 LSP impacts, which may be attributed to the stiffness of CS and need to be confirmed by further increasing LSP impact times.

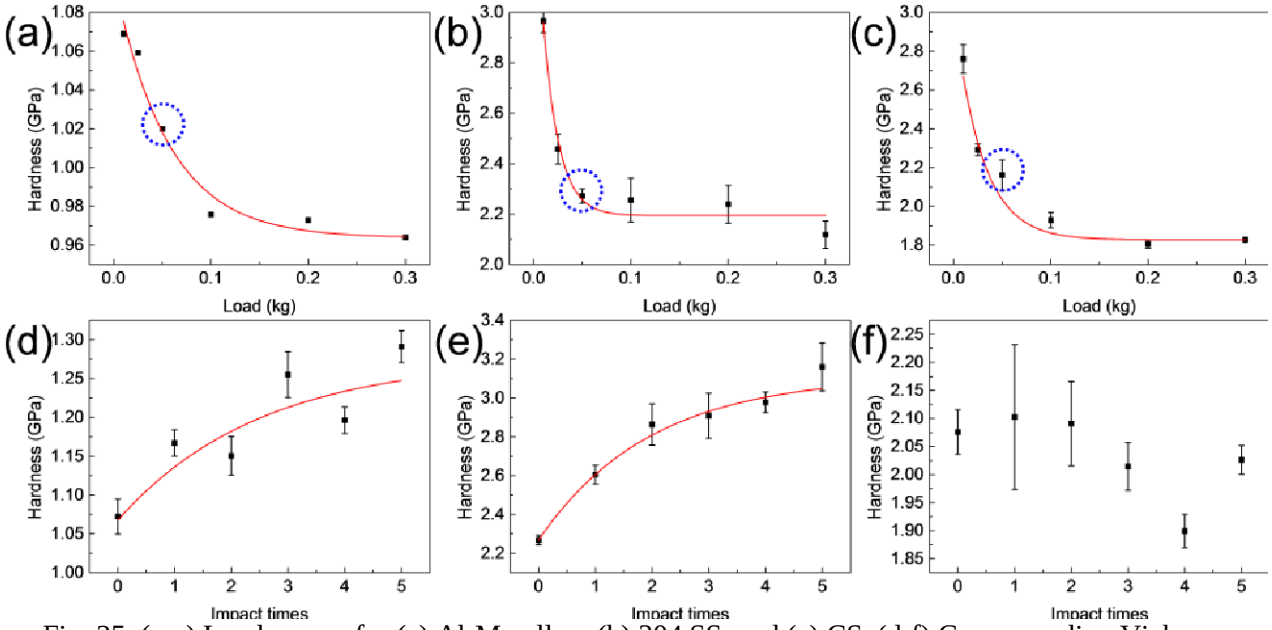

Fig. 25. (a-c) Load curves for (a) Al-Mg alloy, (b) 304 SS, and (c) CS. (d-f) Corresponding Vickers micro-hardness as a function of LSP impacts for (d) Al-Mg alloy, (e) 304 SS, and (f) CS.

To examine the detailed effect of LSP, microhardness distributions of 304 SS and CS samples along the surface direction and the depth treated by single spot and large area LSP were systemically investigated by Tukon 2500 Vickers hardness tester.

3D Microhardness distribution after single-spot LSP

304 SS sample was firstly processed by single spot laser shock peening for 1 to 5 impact times.

Figures 26(a-d) shows the surface morphologies of the single spot LSP induced dents with (a) 1, (b) 2, (c) 3, and (d) 5 impact times, respectively. After LSP, to obtain the cross sections across the center of the LSP induced dents, cutting, grinding, and polishing as described in the sample preparation part were performed to remove part of the sample. The surface morphologies of the samples after cutting, grinding, and polishing are shown in Figs. 26(e-h), corresponding to the images in (a-d). The dependence of dent depth on pulsed laser impact time for 304 SS before and after cutting are shown in Fig. 26(i) and 26(j), respectively. With 1, 2, 3 impacts, the dent depths nearly remain the same value, indicating good cross section location near the dent centers. With 5 LSP impacts, the dent depth decreases a little, showing a small deviation of the cross section location from the dent center.

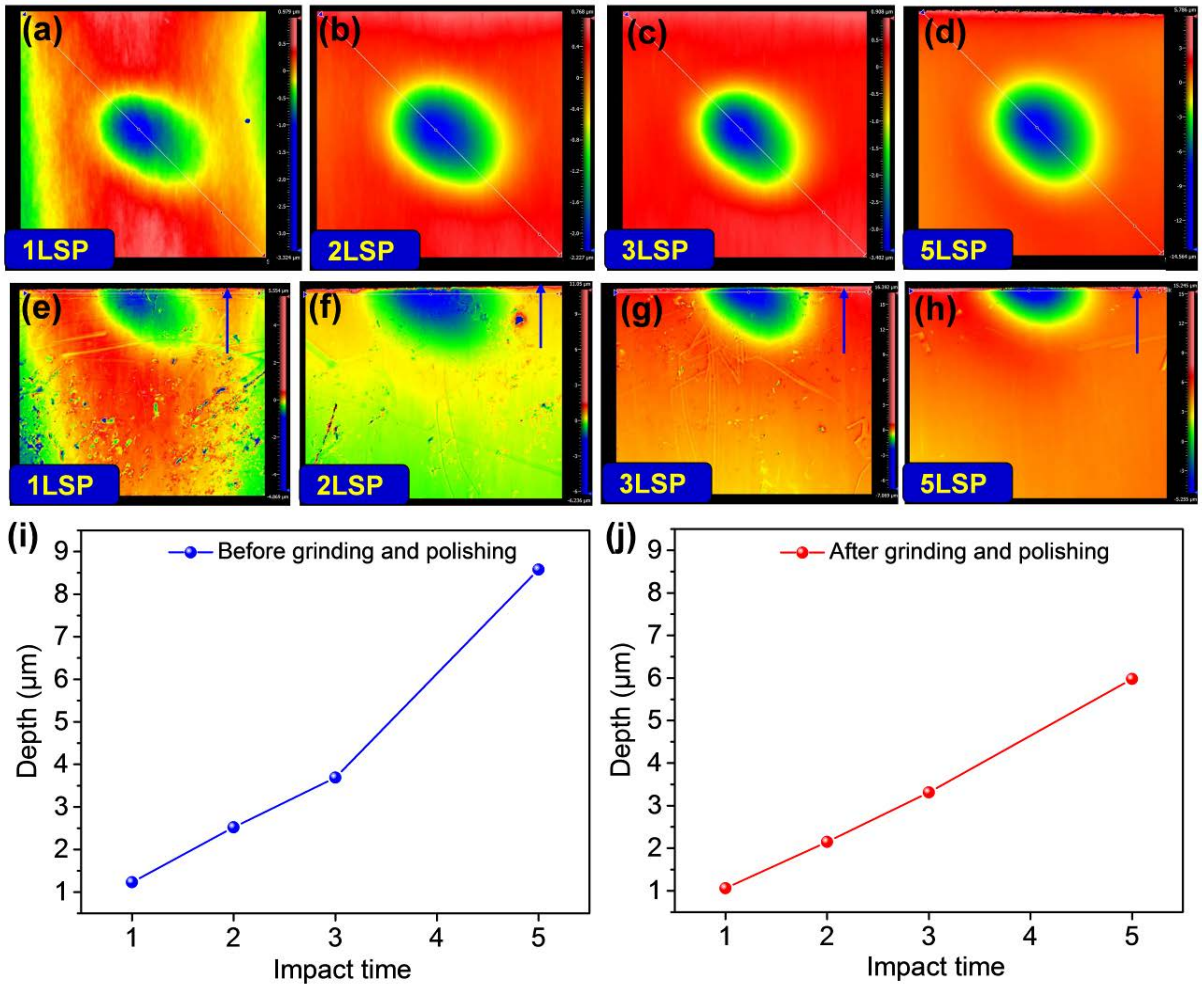

Fig. 26. (a-d) 3D surface topographies of the 304 SS surfaces treated by single pulse LSP for (a) 1, (b) 2, (c) 3, and (e) 5 impacts. (e-h) The corresponding 3D surface topographies of 304 SS in (a-d) after cutting, grinding, and polishing along the near-center line of laser-peened region. The arrows in (e-h) points to the edge of the samples. Dependence of dent depth on pulsed laser impact time for 304 SS (i) before and (j) after cutting, grinding and polishing.

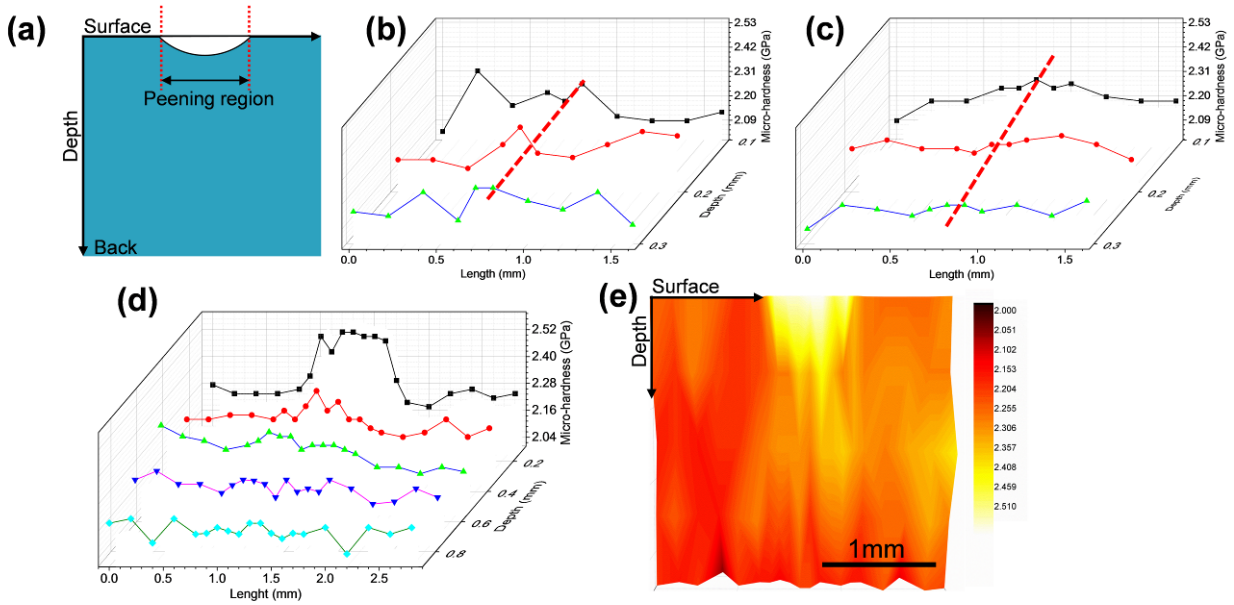

Fig. 27. (a) Schematic of the cross section of 304 SS sample treated by single spot LSP. The single spot micro-hardness distribution along surface and depth treated by single spot LSP for (b) 2, (c) 3, and (d) 5 impacts. (e) 3D cross-sectional micro-hardness distribution treated by single spot LSP for 5 impacts.

After finding the cross section position located along the center line of the LSP-induced dents, the cross-sectional micro-hardness distribution were measured by Vickers micro-hardness tester. As shown in Fig. 27(a), both the hardness distribution along the surface direction and the depth were obtained to generate the two-dimensional (2D) micro-hardness distribution on the selected cross section region. The micro-hardness distribution results for 2, 3, and 5 LSP impacts are shown in Figs. 27(b), (c), and (d), respectively. It can be seen that the highest hardness is obtained near the laser-peened surface (100 μm depth) and with 5 LSP impacts. There is no obvious micro-hardness improvement for the 2 and 3 LSP impacts. Figure 27(e) shows the 3D cross-sectional micro-hardness distribution mapping treated by single spot LSP for 5 impacts, indicating a clear hardness distribution along the surface and depth direction, where the top-surface and center of LSP-induced dent have the maximum values of micro-hardness. In general, the micro-hardness increases with the increment of LSP impact time and decreases rapidly with increased depth.

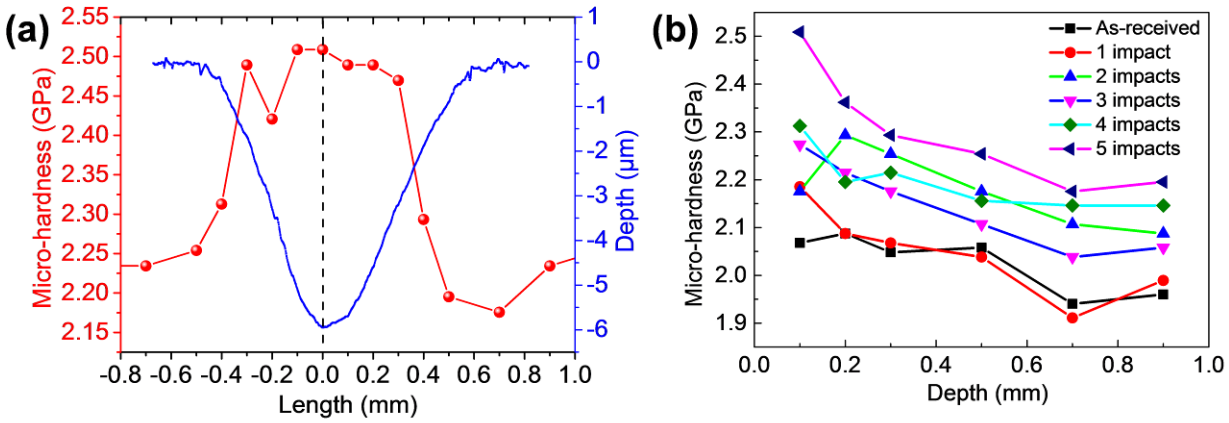

Fig. 28. (a) The micro-hardness distribution along the near-surface and dent depth treated by single spot LSP for 5 impacts. (b) Micro-hardness profiles of 304 SS along the depth direction after multiple LSP impacts with the impact time.

In Fig. 28(a), the profiles of the dent depth and the corresponding cross-sectional hardness distribution along sub-surface (100 μm depth) with 5 single spot LSP impacts are put together for comparison, with the dashed black line indicating the dent center. The dent depth is nearly a Gaussian profile with the center depth of about 6 μm and the diameter of about 1.2 mm. On the other hand, the micro-hardness distribution shows a flat top close to the dent center with a length of about 0.6 mm, and the micro-hardness increases sharply from substrate value to the highest value within 0.2 mm on each side. Figure 28(b) shows the micro-hardness distribution along depth for the 304 SS sample along the depth direction after multiple LSP impacts. It can be observed from Fig. 28(b) that the significant and maximum micro-hardness mainly exists in the sub-surface region for different LSP impacts. Increasing LSP impacts has remarkably improved the microhardness at different depths from 100 to 900 μm, while the values with 1 LSP and 2 LSP have some deviation. Since the micro-hardness value at 900 μm is still higher with LSP compared to as-received sample, the depth affected by single spot LSP must be deeper than 900 μm, which need to be confirmed by hardness profiles at deeper positions and repeated experiments in the future research work.

3D Microhardness distribution after large-area LSP

In this section, the cross-sectional microhardness distribution of the samples after large-area laser shock peening have been investigated.

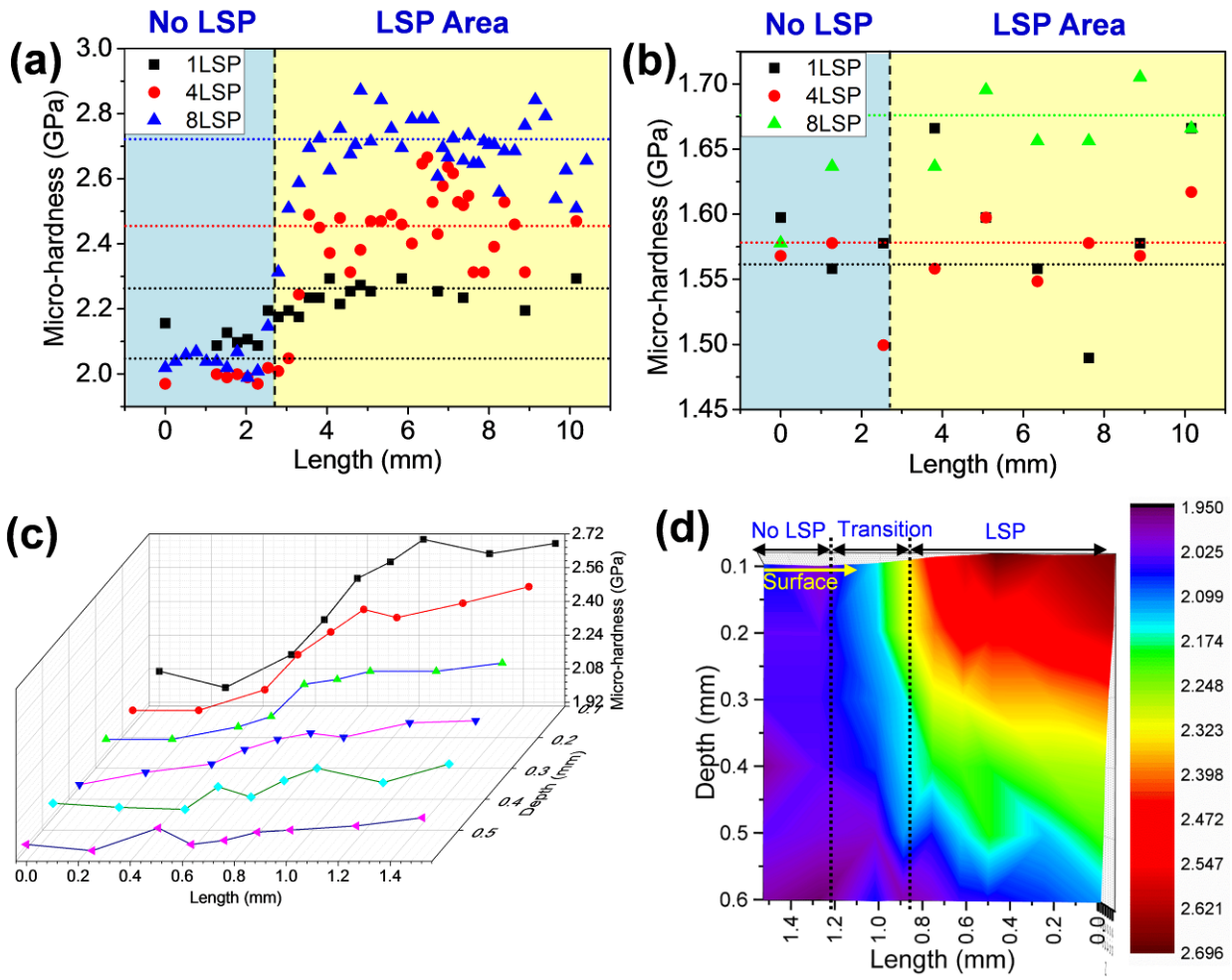

Fig. 29. Micro-hardness distribution of (a) 304 SS and (b) CS along the near-surface from none LSP area to LSP with the impact time. (c) 2D and (d) 3D cross-sectional micro-hardness distribution along depth across the transition area (from No LSP area to 8 LSP area).

Figure 29 shows the micro-hardness distribution along sub-surface direction (at 100 μm depth) for (a) 304 SS and (b) CS. In Fig. 29(a), the micro-hardness of 304 SS shows an obvious improvement from the no-LSP area to the LSP area. In addition, with the increment LSP impact times, the micro-hardness increases rapidly. For 1, 4, and 8 LSP impacts, the average micro-hardness are 2.24, 2.47, 2.70 GPa, respectively, which are approximately 1.1, 1.2, 1.3 times higher than that of no-LSP area (2.04 GPa). In the LSP area, although the laser spot size is 1 mm, the micro-hardness does not show obvious periodical fluctuation, which means relative uniform processing effect could be achieved at the selected overlapping rate of 50%. The uniform micro-hardness distribution might also be related with the flat top hardness phenomena that we observed in the single spot LSP experiment. For CS results in Fig. 29(b), the increase of hardness is not obvious under the same LSP conditions we used for 304 SS. The original average mico-hardness of the CS is only approximately 1.57 GPa, which is much lower than that of the as-received 304 SS (2.04 GPa). After 1, 4, and 8 LSP impacts, the average micro-hardness is

increased to 1.58, 1.59, and 1.67 GPa, respectively. It should be noted that, compared to the 304 SS with higher hardness, the CS with lower hardness is much less hardened by laser shock peening under the same processing parameters. The microstructure like the grain size and phase difference might be the reason, which will be explained by metallographic investigation.

Due to the significant hardness increase of 304 SS by 4 LSP and 8 LSP, the transition from no-LSP area to LSP area could be identified. The length of the transition area with 4 large area LSP is approximately 200, which is similar to that with 5 single spot LSP impacts. For 8 LSP, the transition area is approximately 400 μm, which is much longer than that with 4 LSP. A detailed cross-section micro-hardness distribution along depth cross the transition area from the No-LSP area to 8 LSP area is shown in Figs. 30(c) and (d). For different depths (less than 0.5 mm), the length of the transition area remains the similar value of approximately 400 μm, while the hardness gap between the LSP and No-LSP area decreases with increased depths. At the depth of 600 μm, no obvious hardness difference could be observed between No-LSP area and 8 LSP area. The above results could be attributed to the expansion of the affected region due to multiple LSP impacts.

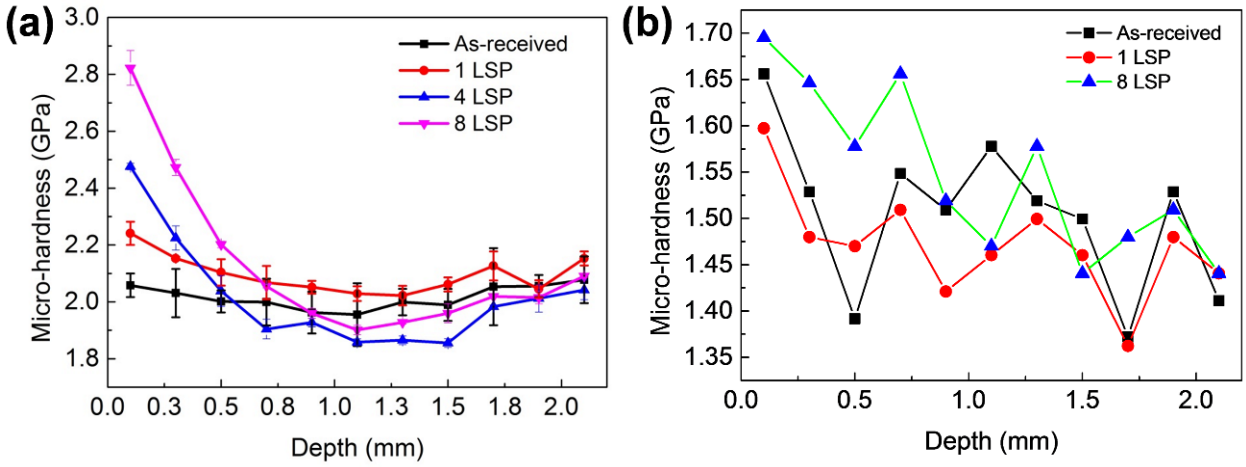

Fig. 30. Micro-hardness profiles of (a) 304 SS and (b) CS after multiple large area LSP impacts with different impact times.

Figure 30 shows the micro-hardness distribution along the depth for (a) 304 SS and (b) CS treated by multiple large area LSP. It can be seen from Fig. 30(a) that, similar to the single spot LSP, the near-surface micro-hardness of 304 SS is the most obviously increased with the increment of LSP impacts, and the micro-hardness decreases rapidly with the increased depth. When the depth is less than 500 μm, the micro-hardness is higher with more LSP impacts. With depth between 500 μm and 700 μm, the LSP-induced hardness improvement vanishes. For deeper position, the magnitude of micro-hardness is not changed and almost not influenced by the impact time. For CS, as shown in Fig. 30(b), the near-surface micro-hardness is increased a little with the increment of LSP impacts, much lower than that of 304 SS. The low micro-

hardness increase of CS confirms the micro-hardness results along the surface direction, which might be induced by the microstructure difference between 304 SS and CS.

(b) Microstructure improvement after LSP

Microstructure investiation is essentially the study of the structural characteristics or constitution of a metal or an alloy in relation to its physical and mechanical properties. Specifically, metallographic examination can provide quantitative information about the specimen grain size, amount of interfacial per unit volume, and the amount and distribution of phases, while TEM can show small structures inside grains. In this project, metallographic observation and TEM are used for microstructure investigation in combination with the micro-hardness results.

Metallographic observation using OM and SEM

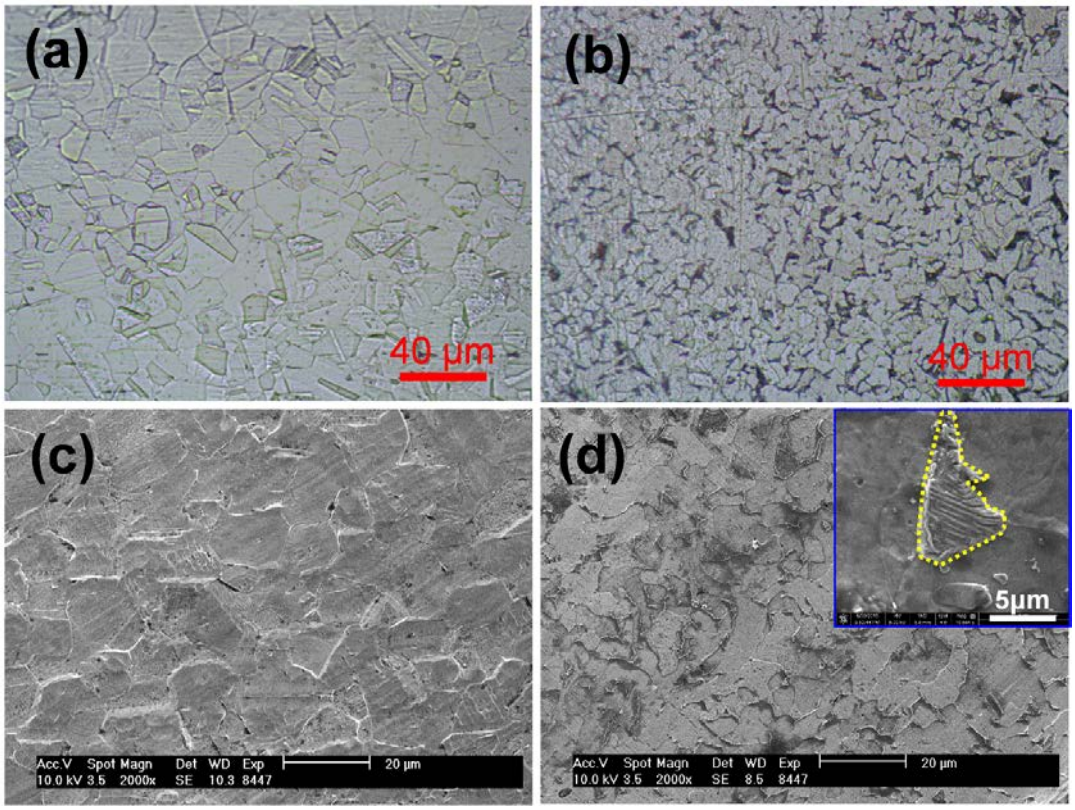

Fig. 31. Optical images of microstructures of original (a) 304 SS and (b) CS after etching. (c) and (d) Corresponding SEM images shown in (a) and (b), respectively. Inset in (d) shows an enlarged SEM image.

For metallographic observation, the polished sample should be etched by special solutions to let the microstructures show up. Aaqua regia and nital were used for 304 SS and CS etching, respectively. After etching, both the optical microscope and SEM were used for imaging. Figures 31(a) and (b) show the optical images of the etched surfaces of 304 SS and CS without laser peening, respectively. The 304 SS sample shows austenite structures (Fig. 31a). CS shows white

ferrite structures with some black areas around the grain boundaries (Fig. 31b), which is suspected to be the secondary phase. To further confirm and identify the micro-structures, SEM observation is needed. Figure 31(c) shows the SEM image of the surface of the etched 304 SS sample, where only austenite structure phase is observed and the average size on the surface is about 11 μm, which is similar to optical imaging results. From the SEM observation (Fig. 31d), the black areas of the CS in optical imaging (Fig. 31b) corresponds to lamellar structures in SEM imaging, which are most likely to be the pearlite. Therefore, CS probably consists of two phases, ferrite and pearlite, respectively. In addition, the existence of pearlite phase is considered to be one of the important reasons for hard-to-change hardness of the CS with LSP.

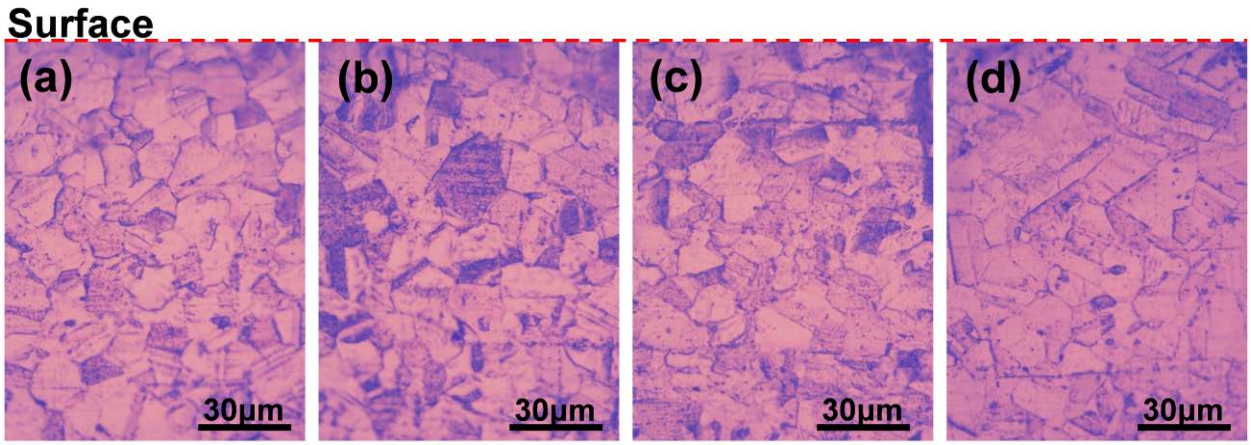

Fig. 32. Optical images of the cross-sectional microstructures of 304 SS (a) before and (b-d) after laser peening for (b) 1, (c) 4, (d) 8 impacts.

Cross section samples after multiple large area LSP impacts were used for metallographic investigation. Figure 32 shows typical optical images of the cross-sections of the 304 SS (a) before laser peening and (b-d) after laser peening for (b) 1, (c) 4, and (d) 8 impacts. The areas used for observation are near the laser-peened surfaces, where the laser peening should be the most effective for micro-structure changes. Figure 33 shows cross-sectional SEM images with different magnification of 304 SS (a-c) before and (d-f) after laser peening for 8 impacts. Grain boundaries are marked by dashed yellow lines in SEM images under the highest magnification (Figs. 33c and f). Compared with the SEM images of the samples before and after laser peening, no obvious changes are observed in the grain size. However, some laminar structures can be clearly observed in the sample treated by 8 LSP impacts, which may be twins generated by shock wave impacts. Through the extended optical and SEM images, the quantitative grain sizes are determined by making lines and counting the intersection numbers. For each grain size achieved, 8 lines at 4 different images are counted. The average grain size of the sample before laser peening is about 10.5 μm, while those after LSP for 1, 4, and 8 impacts are 9.84, 8.9, and 8.82 μm, respectively. Although the grain size does not show great changes, other factors like the increase of twin and dislocation density also contribute to micro-hardness increase we have

measured. On the other hand, the small change of the grain size might be attributed to the low laser power density. Laser with higher pulse energy and better focusing system should be used in the future to enhance the laser shock peening effects.

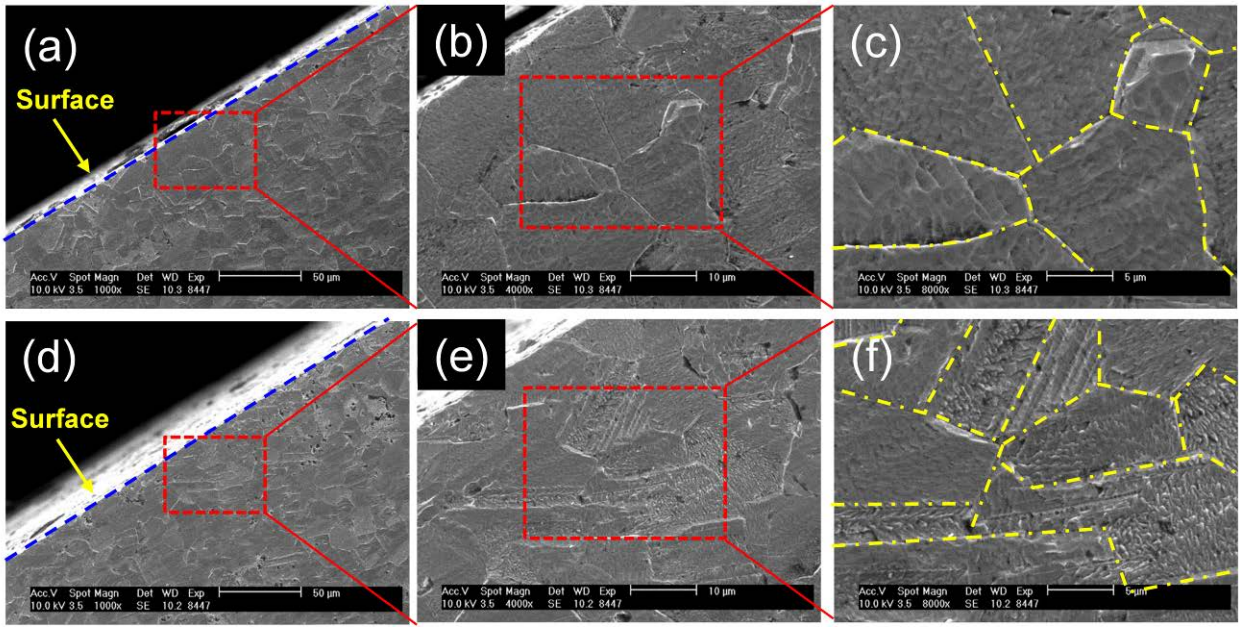

Fig. 33. Different magnified SEM images of the cross-sectional microstructures of 304 SS (a-c) before and (d-f) after laser peening for 8 impacts.

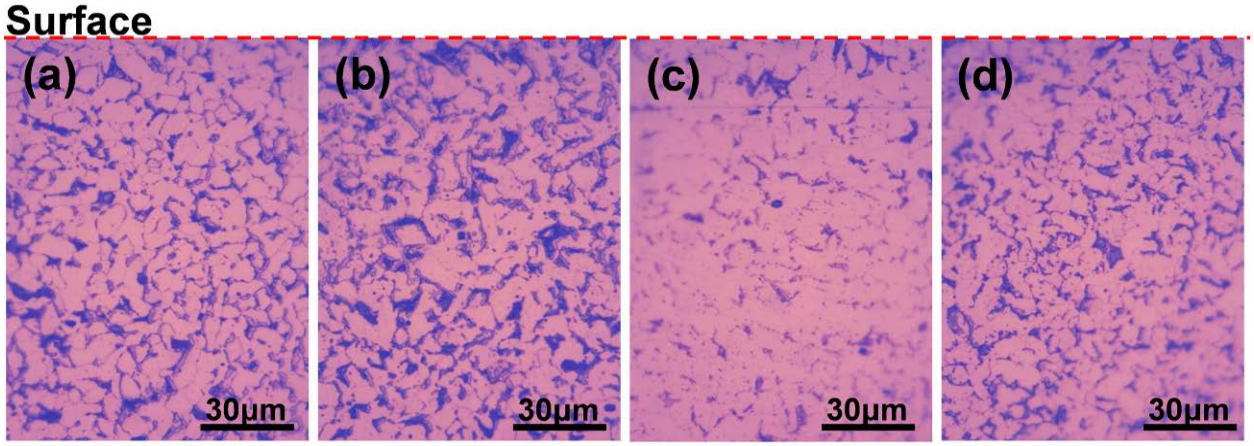

Fig. 34. Optical images of cross-sectional microstructures of CS (a) before and (b-d) after laser peening for (b) 1, (c) 4, (d) 8 impacts.

Figure 34(a) shows the optical images of CS (a) before laser peening, and Fig. 34(b-d) shows the optical images of with (b)1, (c)4 and (d)8 LSP impacts. Figure 35 shows the SEM images with different magnification for 304 SS (a-c) before and (d-f) after laser peening for 8 impacts. The dashed yellow lines in the SEM images with the highest magnification indicate the grain boundaries. Through the same way we did for 304 SS, the average grain size (only for the ferrite) of CS is determined as 6.63 μm before laser peening, and decreases to 6.36 μm after 8 LSP

impacts. The nearly unchanged grain size of the CS agrees well with the tiny change of the micro-hardness before and after LSP processing. Moreover, the grain size of CS that is much smaller than that of the 304 SS might be another reason for the barely changed hardness even with 8 LSP impacts.

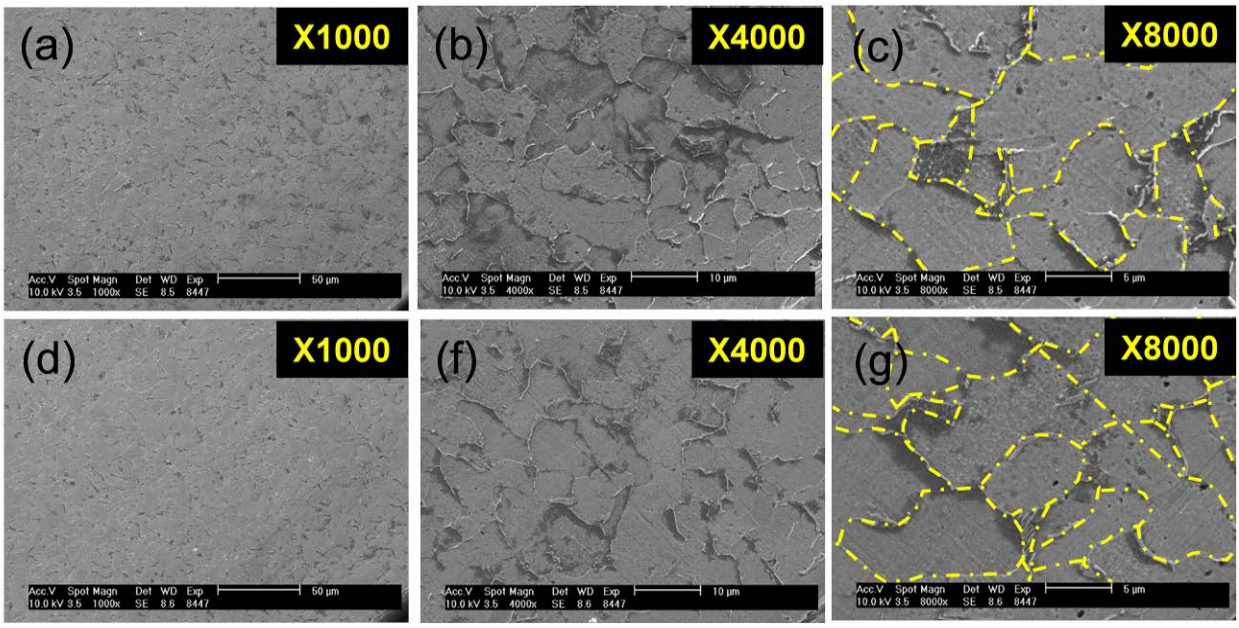

Fig. 35. Different magnified SEM images of cross-sectional microstructures of CS (a-c) before and (d-g) after laser peening for 8 impacts.

TEM observation

After laser peening, different sorts of defects would generate inside the grains of the metal/alloy samples, which have direct relationship with residual stress and the SCC resistance. TEM is the most effective method to observe the small structures/defects inside the grains such as dislocations, stacking faults, and twins. Since the TEM sample preparation and observation are quite complicated and time-consuming, we only use it for comparing the 304 SS samples without and with large-area LSP for 8 impacts. The laser-peened surface were observed, which are expected to show the most obvious micro-structure changes according to the micro-hardness measurement results.

Figure 36 shows some typical TEM images of the grains of the as-received 304 SS sample in the surface layer, in which few microstructure features can be identified. In Fig. 36 (a), an intersection of three grain boundaries is shown, in which most of the areas are free of defects and some point defects exist near the grain boundaries. In Figs. 36 (b) and (c), some stacking faults and dislocations appear. In comparison, TEM images of the surface of the 304 SS sample after 8 LSP impacts are displayed in Fig. 37. Fig. 37 (a) shows the intersection of three grain boundaries, where many black lines appear and they are especially intensive around the boundaries. These

structures should be the increased amount of dislocations. In Fig. 37 (b), some lamellar structures with width of 200 to 300 nanometers are observed, which are suspected as twins. However, electron diffraction pattern are needed to confirm it in the future. In Fig. 37 (c), plenty of stacking faults are observed. In conclusion, three typical deformation-induced microstructural features are identified in 304 SS sample subjected to 8 large-area LSP impacts: dislocations, twins, and stacking faults. The defect generation such as the dislocation density increase will result in the increase of hardness and compressive residual stress, which confirms the micro-hardness results we have measured.

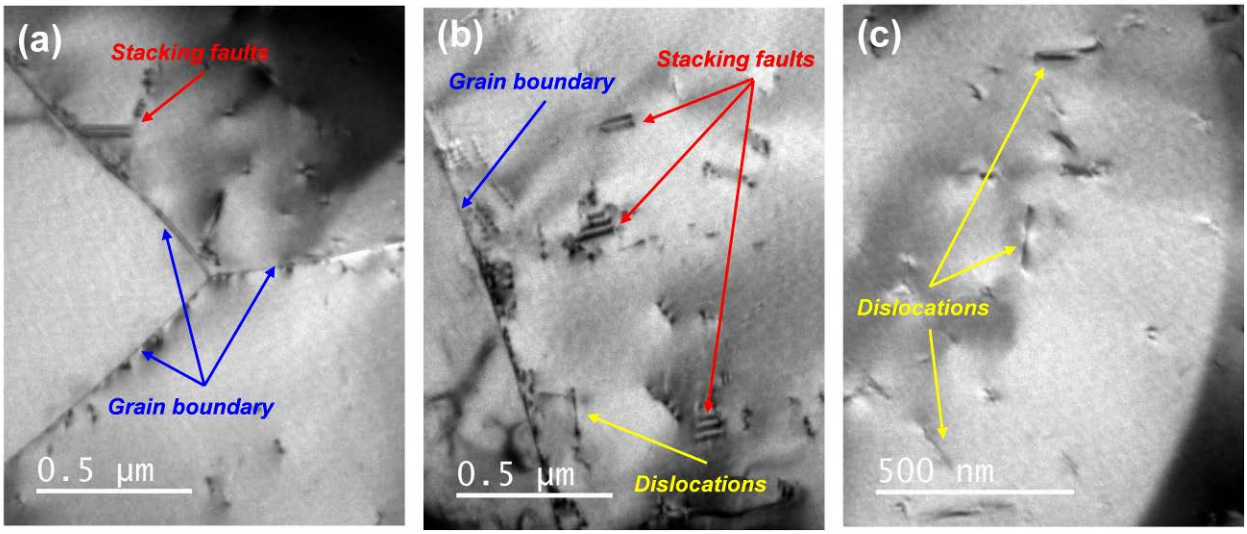

Fig. 36. Typical TEM images of 304 SS without laser peening.

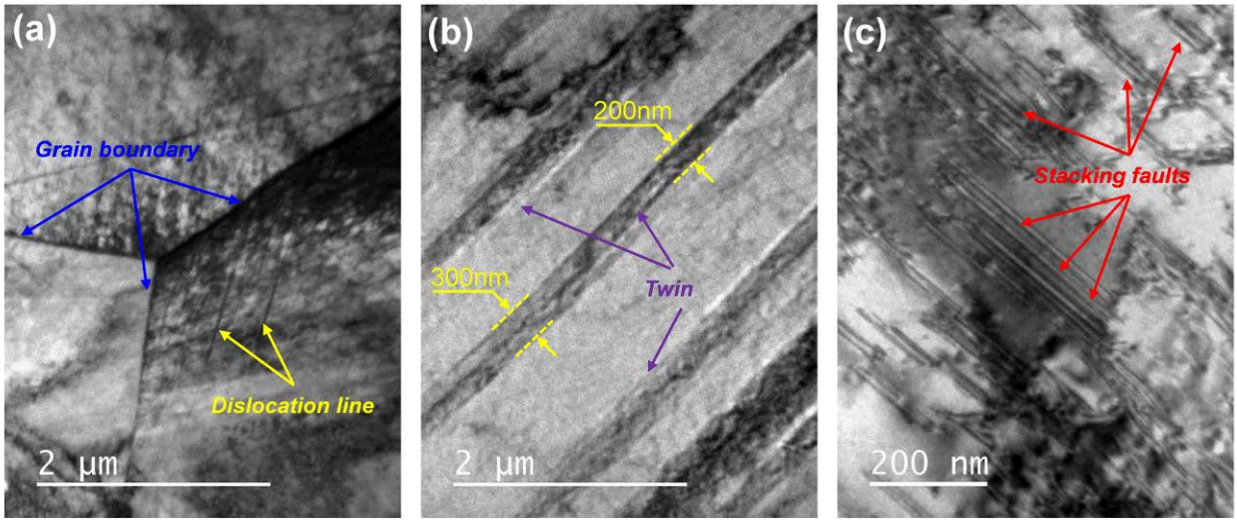

Fig. 37. Typical TEM images of 304 SS subjected to 8 LSP impacts.

(c) Stress corrosion cracking (SCC) resistance improvement after LSP

SCC constant load test setups and procedures

A number of experimental procedures have been developed to assess susceptibility to SCC. Results from these tests can be used to compare SCC susceptibility of different metals. One of the most widely used SCC assessment methods is the uniaxial constant load test which is conducted in accordance with NACE-TM-0177. In this project, both the sample preparation and practical tests have been done.

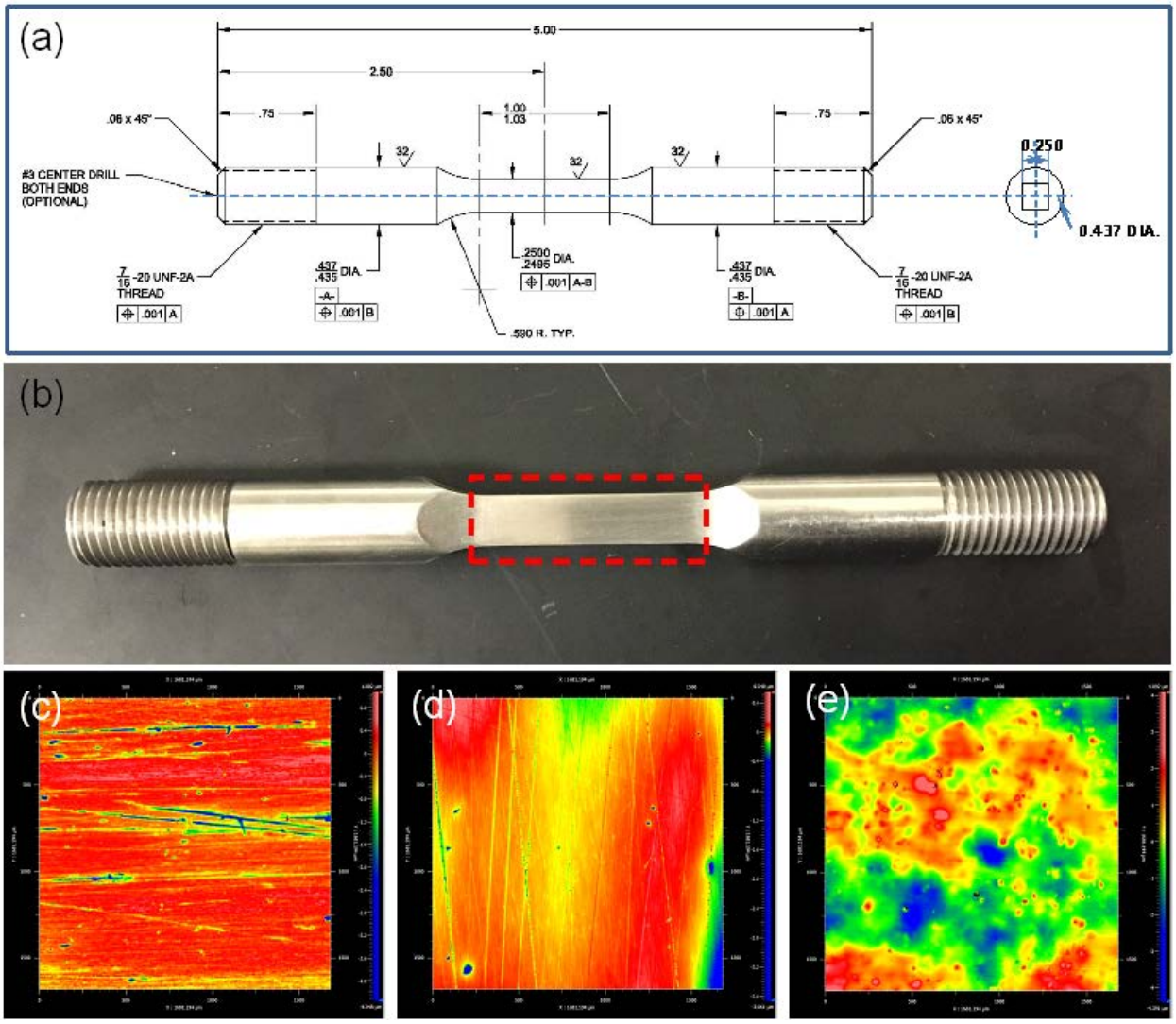

Fig. 38. The (a) drawing and (b) actual 304 SS sample for SCC tests. (c) 3D surface topographies of 304 SS sample (c) before polishing, (c) after mechanical polishing, and (e) after electrochemical polishing. (Roughness for (c-e) are 266, 69, 863 nm, respectively.)

Firstly, the sample in the round dog-bone shape was manufactured by 304 SS according to the drawing shown in Fig. 38 (a). Figure 38 (b) displays a photograph of actual test sample.

Secondly, the testing area marked with dashed red lines was processed in turn by mechanical polishing to remove the large scratches and electrochemical polishing to remove the small defects and surface residual stress. Typical surface morphologies of test samples before polishing, after mechanical polishing, and after electrochemical polishing are shown in Figs. 38 (c), (d), and (e), respectively. The surface roughness is decreased from 266 nm to 69 nm after mechanical polishing. However, after electrochemical polishing, the surface roughness increased to 863 nm. It should be note that the sample surface after electrochemical polishing was even more shining while there were some newly developed dents resulting in roughness increase. Thus, the electrochemical polishing works to remove small scratches, but it needs to be further optimized (solution composition, temperature, current, and polishing time) to avoid generating defects itself and get a better surface.

An initial SCC test was conducted using 304 SS sample without laser peening. The sample was installed in the proof ring and tested with a simulated environment: test solution consisting of 44.2% $MgCl_2$ dissolved in distilled water at boiling temperature of 144°C and with applied stress of 300 MPa. After 48 hours, the sample was taken out of the proof ring and characterized using optical microscope. Two typical corrosions are observed on the testing area: pitting and SCC cracking, as shown in Figs. 39 (b) and (c). A close examination reveals that the SCC crack initiates at the pitting points and propagates perpendicular to the applied stress, indicating that corrosion pits are the main potential sites for surface crack formation. The stress concentration in the pit will give rise to crack formation and subsequent propagation. Since the SCC cracking have been initiated within 48 hours under the selected conditions, we can make use of the current condition for further SCC test and investigation of the effect of laser peening on SCC.

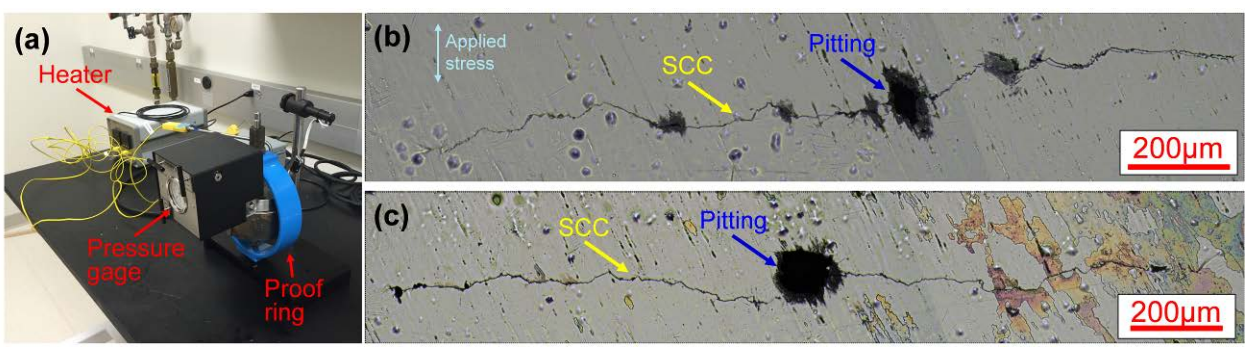

Fig. 39. (a) Experimental setup of proof ring for CLT tests. (b) and (c) Two typical optical images of original 304 SS sample with SCC test load of 300 MPa and duration of 48 h, which show pitting and SCC cracks.

Crack/microstrocture analysis after SCC constant load test

The constant load test results of the 304 SS sample with and without laser peening were investigated. Before the SCC test, large-area laser shock peening by a Nd:YAG laser (850 mJ pulse energy, 50% overlapping rate, 4 times) was performed on two adjacent faces of the 304 SS sample, while the other two faces were not laser peened. After the SCC test for 96 hours, an optical microscope was used to investigate the effect of laser peening on corrosion resistance. It was found that, due to the long testing time, several cracks had formed on both laser-peened and non-laser-peened 304 SS sample surfaces. However, the density (or the number) of cracks formed on each surface of the testing area were different, summarized in Table 3. The numbers of cracks formed on two laser-peened surfaces (Faces 1 and 2) were 6 and 11, respectively, which was significantly less than those formed on the two non-laser-peened faces (20 and 48). The decline in the number of cracks on laser-peened surfaces indicated the improved SCC corrosion resistance of laser-peened 304 SS samples.

Table 3. The number of cracks formed on different surfaces of the SCC testing sample.

Face 1 (laser peened)	**Face 2 (laser peened)**	**Face 3 (not laser peened)**	**Face 4 (not laser peened)**
6	11	48	20

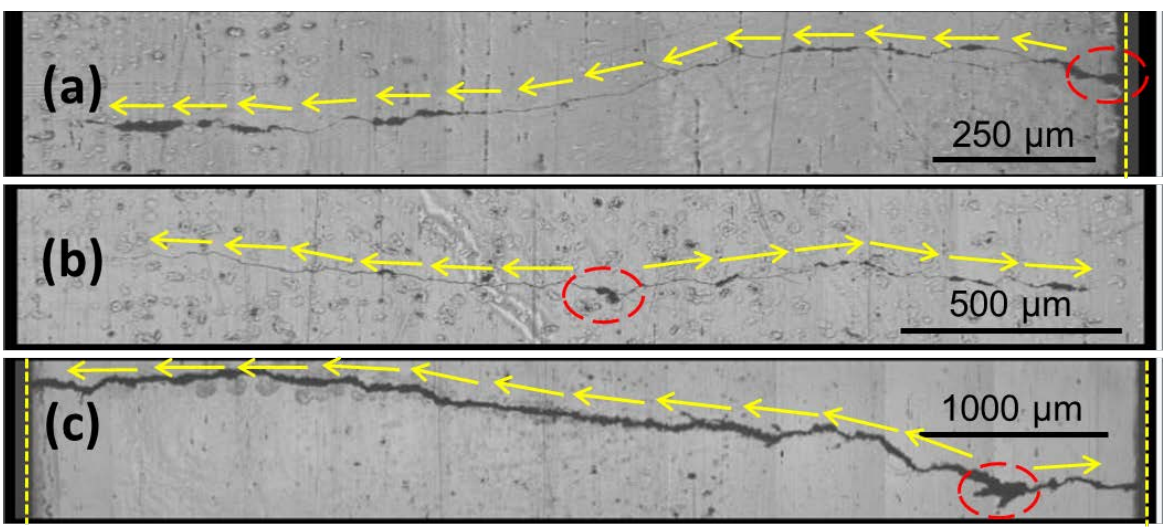

Fig. 40. Typical optical images of cracks formed on the 304 SS sample surface after SCC testing with a load of 300 MPa and a test time of 96 hr. (a) The crack originated from the edge of the test face; (b) the crack formed inside the test face; (c) a crack growing through the test face. The yellow dashed lines indicate sample edges, the red circle indicates the starting point, and the yellow arrow indicates the direction of the crack growth.

A careful observation through an optical microscope revealed that the cracks generated could be classified into three types, as shown in Fig. 40. A Type 1 crack was formed that originated from

the edge of the sample and grew into the face (Fig. 40 (a)). Type 2 (Fig. 40 (b)) and Type 3 (Fig. 40 (c)) cracks were both formed originating from the inside faces and growing outward to the edge. The difference is that the Type 3 crack grew longer, reaching the sample's edges. On the non-laser-peened surfaces, all three of the kinds of cracks were observed; while on the laser-peened surfaces, only the first kind of crack appeared. The cracks generated on the laser-peened faces might have been induced by the crack expansion from the none-laser-peened surfaces. This phenomenon also indicated the relatively low corrosion resistance on the sample edges, which should be attributed to the unconfined structure and, consequently, low compressive residual stress induced by laser peening.

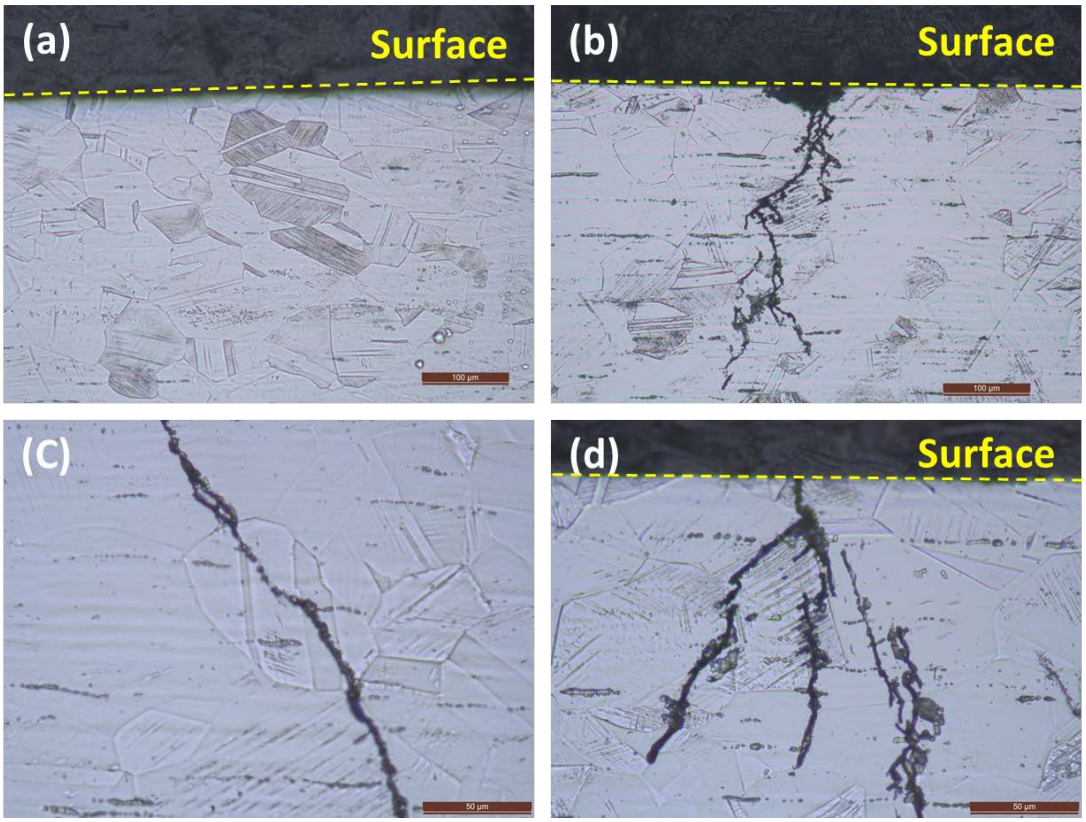

Fig. 41. Typical cross-sectional metallographic images of 304 SS samples after SCC test with a load of 300 MPa and a test time of 96 hr. (a) Crack-free area, (b-d) crack area with different kinds of cracking: transgranular crack (c), (b, d) branched cracks.

The cross-sectional metallographic investigation was performed to further investigate the cracks induced by SCC. Figures 41(a) and 41(b) show the typical metallographic images of 304 SS samples (a) with and (b) without stress corrosion cracking, respectively. In Fig. 41(b), pitting could be observed on the surface, which is the starting point for stress corrosion cracking, and it grew inside the sample toward the center. The crack passed through several grains, indicating that it was a transgranular crack. An obvious transgranular crack was also observed, as shown in

Fig. 41(c). Figure 41(d) shows another kind of crack, where some small tips protruded from the main crack, grew along the grain/twin boundary to the beginning, and then spread through the grains to form a bigger branched crack. It should be pointed out that the directions in which the crack grew along the surface and the depth are all perpendicular to the applied tensile stress direction, which should be the main factor in the cracks's growth and the cause of the transgranular crack type.

2.2.2. Laser shock peening with low energy Nd:YAG laser

2.2.2.1. Low energy Nd:YAG laser peening setup and procedures

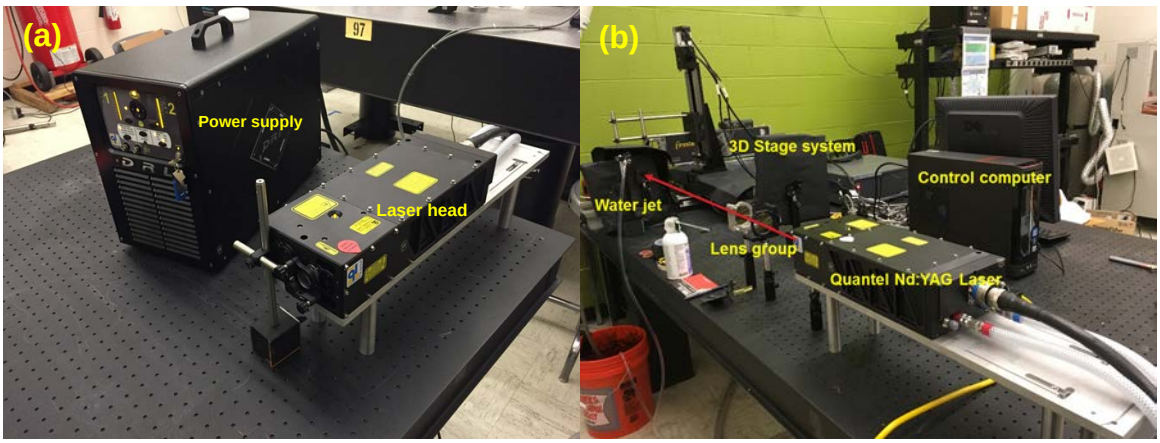

Fig. 42. Newly designed Nd:YAG laser peening system

To reduce the equipment size, weight, and complexity, a new LSP system was established using a low energy compact Quantel Nd:YAG laser (DRL650) and a programmable 3D stage, which is a test system for the portable laser peening equipment in the future. In Fig. 42a., the weight of the laser is light, with a 6.4 Kg laser head and an 18 Kg power supply. The size of the laser system is also very compact: the laser head measures only 94 × 432 × 160 mm, while the power supply is 406 × 236 × 500 mm. The laser head is completely sealed and filled with high pressure gas allowing it to operate in harsh environments, such as underwater, high humidity, and serious vibration. The main parameters of the laser are: 1064 nm wavelength, 650 mJ maximum pulse energy, 15 ns pulse duration, 6.5 mm output beam diameter, and 1-30 Hz repetition rate. Although the laser repetition rate could be set from 1 to 30 Hz, we only used 5 Hz to avoid the incident laser from being seriously disturbed by the water spray induced by previous laser impacts. The entire laser peening system is shown in Fig. 42b. The sample was held by a 3D stage controlled by a computer to realize the scanning path and speed needed. The water jet was fixed to the stage to keep the water film stable on the sample surface while the stage was moving. A blower was used to prevent water sprays from reaching the optics. Two kind of optical designs are shown in Fig. 43. For both of them, a plano-concave lens was used to expand the laser beam diameter followed by two plano-convex lens to collimate and focus the laser

beam. The laser spot diameter after focusing could be varied by changing the lens group setup and the designs achieved two different focused spot diameters: 2.2 mm and 1.4 mm. Considering the influence of the sacrificial coating, laser shock peening with 100 µm black tape without any coating were tested. The details of the laser parameters/confining layer/ sacrificial coating are shown in Table 4.

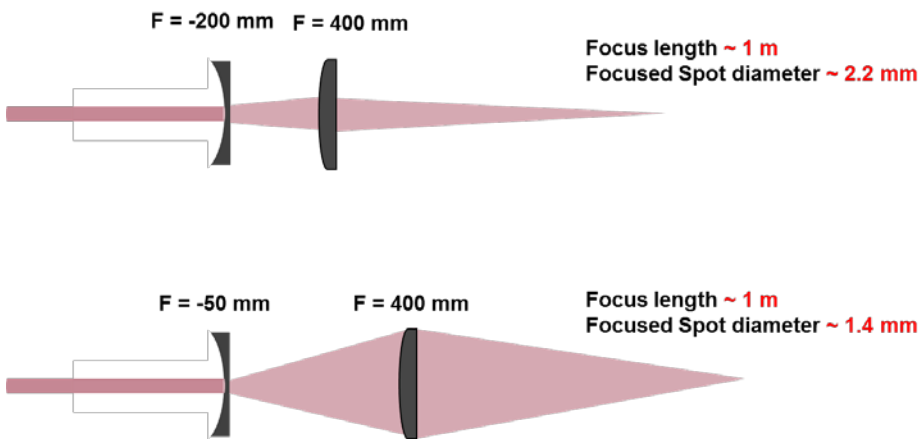

Fig. 43. Schematic of the two kind of optical designs

Table 4. The processing parameters used in low energy LSP experiments

Laser system	Quantel DRL650 laser; Wavelength: 1064 nm; Pulse energy: 650 mJ; Pulse duration: 15 ns; Frequency: 1-30 Hz; Spot size after focusing: 2.2 or 1.4 mm
Confining layer	Water jet with a layer thickness of approximately 1 mm
Sacrificial coating	Black tape (~100 µm) or no sacrificial coating

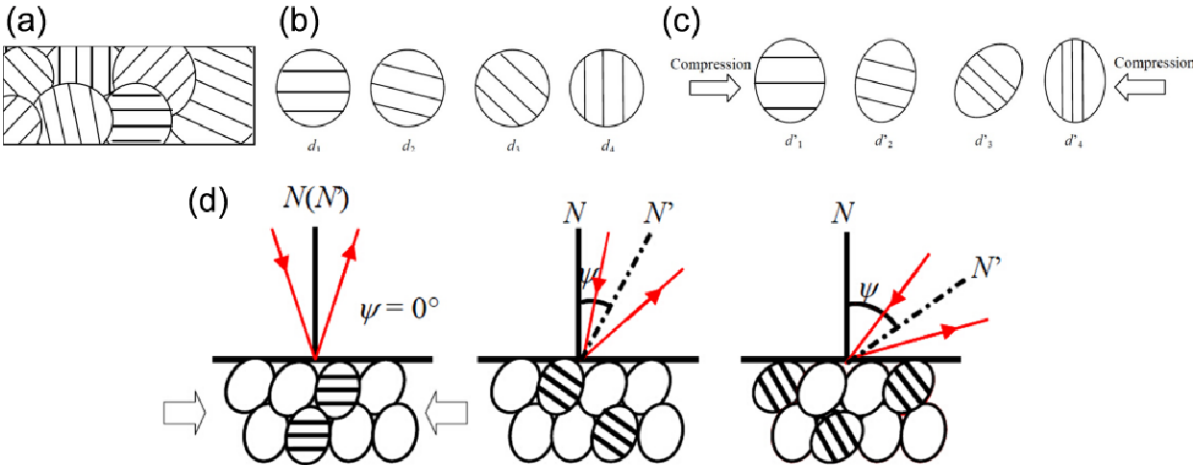

Fig. 44. Schematic of crystal oriented in (a) random directions in polycrystalline material, (b) different crystal orientation under Stress-free condition, (c) and after compressive stress with plastic deformation (c). (d) XRD theory model for residual stress measurement.

In this section, residual stress was investigated in details to reflect the influence of low energy LSP. Compressive residual stress is an important characterization for metal corrosion, since it could effectively prevent crack generation on the protective oxidization layer on metal surface and thus increase the corrosion resistance significantly, especially for stress corrosion cracking. The residual stresses after LSP processing were determined using a non-destructive technique, X-ray diffraction (XRD) $\sin^2\psi$ method. The principle of X-ray diffraction $\sin^2\psi$ method is shown in Fig. 44. As we know, metals are polycrystalline materials composed of numerous crystal particles oriented in random directions (Fig. 44a). Under stress free condition (Fig. 44b), lattice spacing d1=d2=d3=d4; after compressive stress with plastic deformation (Fig. 44c), d1>d2>d3>d4. This lattice spacing change at different directions reflects the residual stress and could be measured by XRD through changing ψ (Fig. 44d).

The surface residual stress measurements were conducted by X-ray diffraction (XRD) equipment (Smartlab, Rigaku) with Cu as the anode target and monochromator for signal filter. The 2-theta angle was selected as 137°, while five incident angles were chosen as -45°, -37.76^o, -30°, -20.7^o, and 0°, respectively. The elastic modulus was selected as 200,000 MPa with a Poisson's rate of 0.29. To obtain the residual stress distribution along depth, electrochemical polishing was used to remove thin layers from the sample surfaces with certain thicknesses.

2.2.2.2. Large spot Nd:YAG laser shock peening experiments

With a large spot of 2.2 mm diameter at the focus point, both single spot laser peening for sample position optimization and large area laser peening with and without black tape were conducted in this section.

(a) Optimization of the sample position

The sample position optimization was first conducted on Al alloy by single spot laser peening. One LSP impact with the pulse energy of 650 mJ was used with 100 µm black tape as the sacrificial coating. The LSP generated dent depth and diameter at different sample positions are shown in Fig. 45a and 45b. The zero position is arbitrary. The dent depth increases from ~ 10 µm to ~ 20 µm with sample position changing from -80 mm to 0 mm, tops at 0 - 30 mm, and decreases slowly from 30 mm to 80 mm with strong variation. In Fig. 45a, the dashed blue square shows that in a large scale of about 100 mm length (-20 to 80 mm), the dent depth remains at a relatively large value (> 18 µm). In Fig. 45b, the dent diameter also shows stability at the same range with the value of approximately 1.8 mm. These results indicate similar shock wave intensity and profile among a large range of sample positons, which should be attributed to the laser characteristics. Different from our previously used Nd:YAG laser with near Gaussian profile, the Quantel laser has a flat top profile, which allows for uniform distribution of laser energy at the cross section view and longer depth of focus (DOF) along the propagation direction.

These two-laser characters result in a more uniform shock wave within a large range of sample position, which means the low energy laser peening system is insensitive to laser-sample distance and therefore beneficial for easy operation in practical environments. The sample position of 20 mm is used in the following sections.

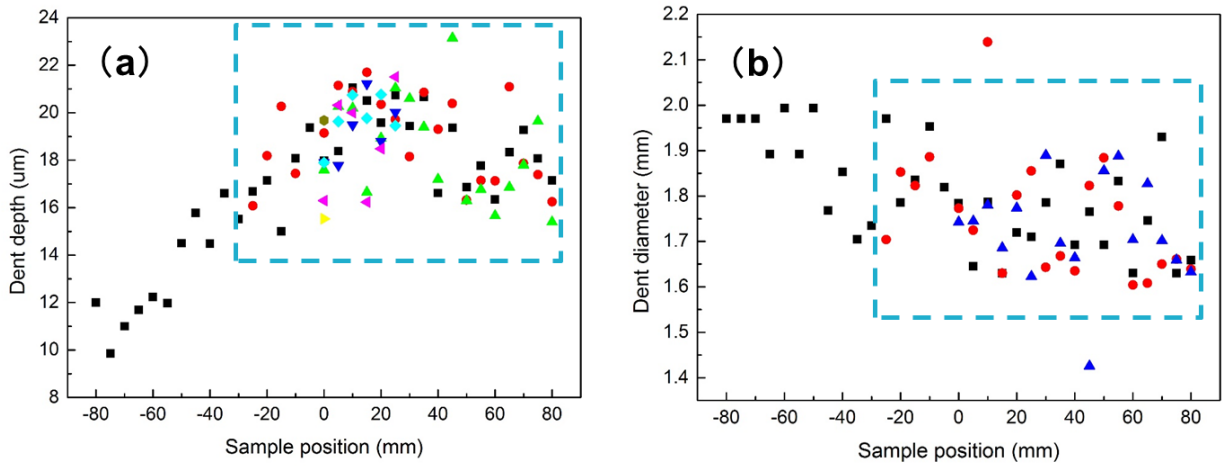

Fig. 45. Laser peening induced (a) dent depth and (b) dent diameter at different sample positions on Al alloy surface.

(b) Large spot laser shock peening with black tape

Large area laser shock peening was carried out with a laser spot size of 2.2 mm diameter on the 1018 CS with black tape as the sacrificial coating. Considering the laser spot shape and diameter, the best spot to spot distance is 0.5/0.8, which means 0.5 mm spot to spot distance along the vertical direction and 0.8 mm along the horizontal direction. The CS was mechanically and electrochemically polished to obtain a stress-free surface and then laser peened for 1 and 2 times. As shown in Fig. 46., without laser peening, the residual stress is - 3.0 ± 25.5 MPa, which increases to - 280.5 ± 10.6 MPa after one laser peening impact and further increases to - 365.8 ± 25.2 after another impact. Thus, for laser shock peening with black tape, the increase of the surface residual stress could be obtained by posting more peening impacts.

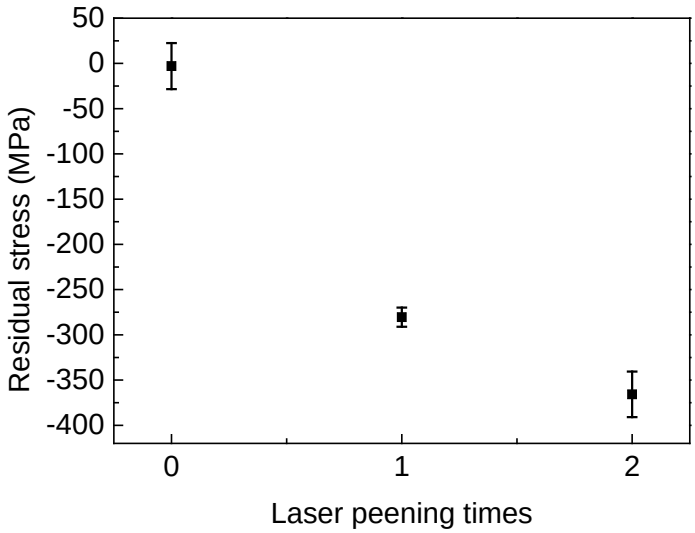

Fig. 46. Surface residual stress of the 1018 CS after laser peening with black tape for different times (2.2 mm spot diameter, 650 mJ pulse energy, 0.5/0.75 spot to spot distance).

(c) Large spot laser shock peening without sacrificial coating

Laser peening without coating (LPwC) is a promising method since it avoids the usage of the sacrificial coatings such as tapes, paints, and Al foils. It not only reduces the cost, but also declines the contaminations generated during the laser peening progress. In order to suppress the laser ablation, LPwC could only be realized by low pulse energy, which is appropriate with the DRL650 Nd:YAG laser. Therefore, LPwC is also carried out in this project besides the normal laser peening.

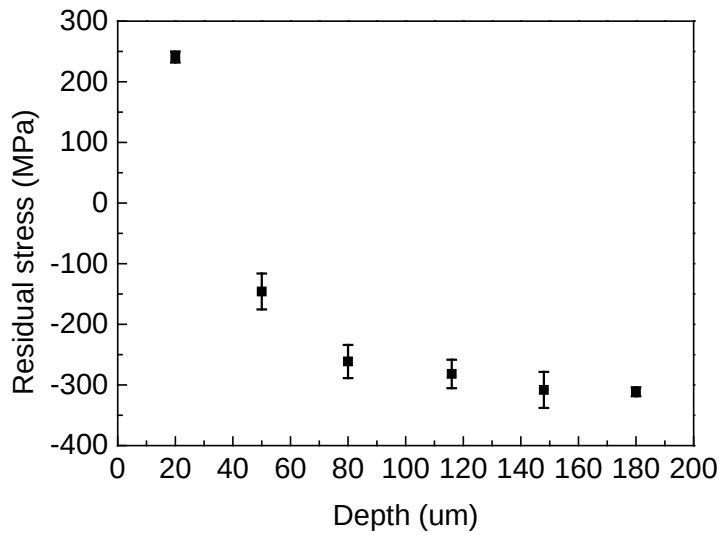

Fig. 47. In depth residual stress distribution of the 1018 CS after laser peening without coating (2.2 mm spot diameter, 650 mJ pulse energy, 0.5/0.75 spot to spot distance, 3 times).

Fig. 47. shows the residual stress distribution of the 1018 CS along depth after LPwC for 3 times with a 2.2 mm spot diameter, a 650 mJ pulse energy, a 0.5/0.75 spot to spot distance. 0.5/0.75 means 0.5 mm spot to spot distance along the vertical direction and 0.75 mm along the horizontal direction. The near surface region has a tensile stress of 241 MPa due to the laser ablation. But the depth of the tensile region is less than 50 µm. At deeper regions, the residual stress becomes compressive, increases to ~300 MPa gradually, and keeps stable within 180 µm. Although the tensile residual stress on the surface is a disadvantage for stress corrosion cracking resistance, the compressive residual stress after 50 µm depth could prevent the corrosion crack tips from further growing into deeper regions. In this aspect, the LPwC is also a possible way to avoid the material and structure failure induced by the stress corrosion cracking in pipeline systems.

2.2.2.3. Small spot Nd:YAG laser shock peening experiments

In this section, a small laser spot of 1.4 mm diameter at the focus point was used both for single spot laser peening (sample position optimization) and large area laser peening with and without black tape.

(a) Optimization of the sample position

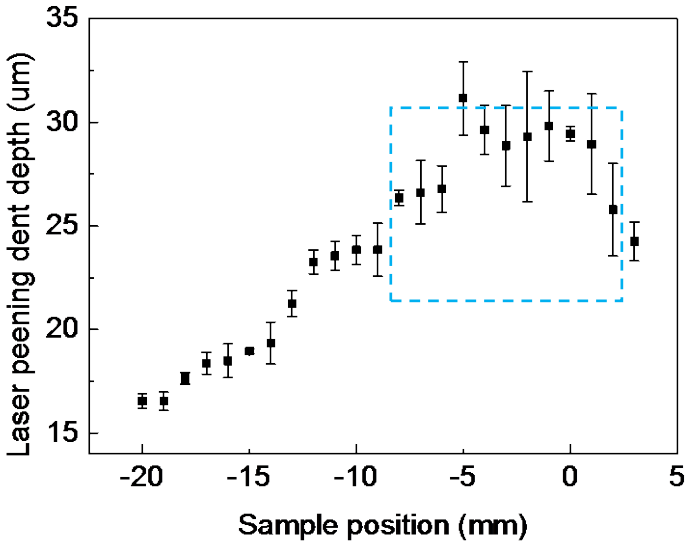

Fig. 48. The dent depth on Al alloy surfaces after laser peening with black tape at different sample positions.

As shown in Fig. 48, the laser peening dent depth was measured on the 1018 CS surface after Nd:YAG laser peening at different sample positions (650 mJ pulse energy, 100 µm black tape, 1 LSP impact). Five repeated spots were measured and averaged for each sample position. The zero point is an arbitrary position. The single spot dent depth varies from 17 µm to 31 µm, and peaks at the sample positions from -8 to 2 mm. With the smaller laser spot diameter of 1.4 mm at the focus point, the dent depth increases enormously to 31 µm compared to the 21 µm dent depth

obtained with the 2.2 mm laser spot size. The increase of the dent depth reflects the increment of the laser induced shock wave intensity due to the decrease of the spot size. On the other hand, the dashed blue square in Fig. 6 shows that in a much smaller scale of only 10 mm length (-8 to 2 mm) where the dent depth remains at a large value (> 26 μm). This phenomenon may also be attributed to the small spot size, which makes the laser induced shock wave easier to attenuate. The sample position of 0 mm is used in the following sections.

(b) Small spot laser shock peening with black tape

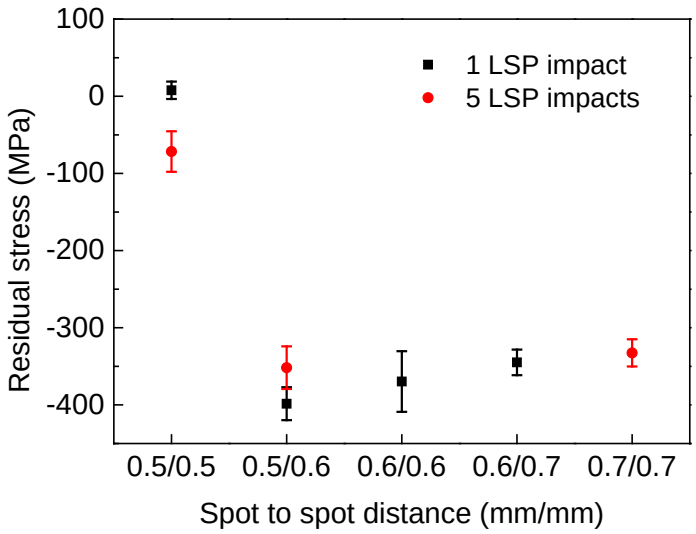

Fig. 49. Surface residual stress of the 1018 CS after laser peening with black tape with different spot to spot distances for different impact times (1.4 mm spot diameter, 650 mJ pulse energy, 1 or 5 times).

Large area laser shock peening was carried out with a laser spot size of 1.4 mm diameter on the 1018 CS with black tape as the sacrificial coating. Fig. 49 shows the effect of different spot to spot distances (0.5/0.5, 0.5/0.6, 0.6/0.6, 0.6/0.7, and 0.7/0.7) and laser peening times (1 and 5 times) on the surface residual stress. Take 0.5/0.6 for example, it means 0.5 mm spot to spot distance along the vertical direction and 0.6 mm along the horizontal direction. After laser peening for 1 time, the surface residual stress becomes compressive except for the smallest spot to spot distance of 0.5/0.5, which is only 7.7 ± 11.3 MPa since the black tape was removed and the sample surface was partly ablated. With larger spot to spot distances of 0.5/0.6, 0.6/0.6, 0.6/0.7, and 0.7/0.7, the compressive residual stress increases slightly from -344.9 ± 16.6 to -398.5 ± 21.3 MPa as the spot to spot distance becomes smaller. After laser peening for 5 times, the surface residual stress becomes compressive with the spot to spot distance of 0.5/0.5 even though the sample surface is ablated. On the other hand, the surface residual stress decreases slightly from -398.5 ± 21.3 to -351.7 ± -27.6 MPa with the spot to spot distance of 0.5/0.6 while the laser peening times increases from 1 to 5. It is considered that the in-depth residual stress increase should be the reason for the decrease of the surface residual stress after repeated LSP impacts.

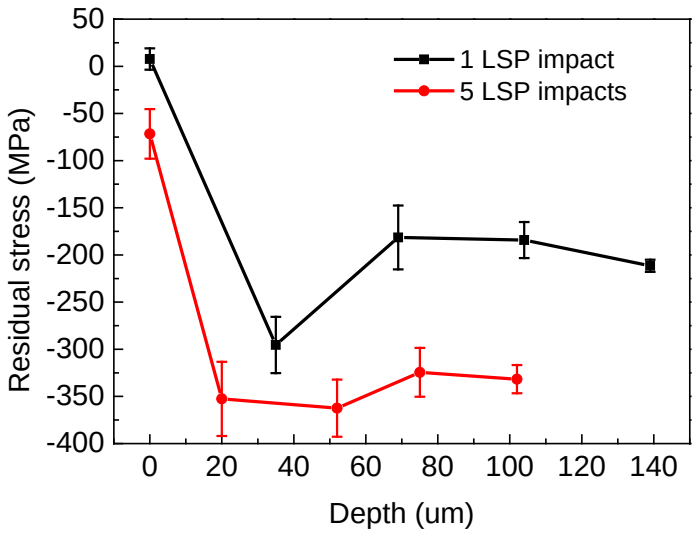

Fig. 50. In depth residual stress distribution of the 1018 CS after laser peening with black tape for different times (1.4 mm spot diameter, 650 mJ pulse energy, 0.5/0.5 spot to spot distance, 1 or 5 times).

The two laser-ablated samples (0.5/0.5, 1 time and 0.5/0.5, 5 times) in Fig. 50 were further investigated for residual stress distribution along the depth. After laser peening for 1 time, as shown in Fig. 50, the residual stress of the sample soon changes from tensile (at the surface) to compressive as the depth increases, peaks at 35 µm depth with -295.5 ± 29.9 MPa, and then decreases to 181.5 ± 33.9 MPa at 69 µm and keeps stable within 140 µm. On the other hands, after laser peening for 5 times, the compressive residual stress increases rapidly from -71.6 ± 26.3 MPa at the surface to -352.6 ± 39.3 MPa at 20 µm depth and then keeps nearly stable within 100 µm. Obviously, the increase of the laser peening times could improve the peak value of the in-depth compressive residual stress. It could also extend the heavily compressive region deeper into the sample. According to the trend of the two curves, it is also reasonable to say that the laser peening affected depth increases with the increment of the laser peening times.

(c) Small spot laser shock peening without sacrificial coating

Laser peening without coating was carried out with a laser spot size of 1.4 mm diameter on the 1018 CS. As shown in Fig. 51., the residual stress distribution along depth was investigated on two pieces of samples after LPwC for one time with different spot to spot distances of 0.5/0.5 and 0.7/0.7, respectively. Take 0.5/0.5 for example, it means 0.5 mm spot to spot distance along the vertical direction and 0.5 mm along the horizontal direction. With the larger spot to spot distance of 0.7/0.7, the residual stress of the sample increases to -232.4 ± 9.6 MPa at 60 µm depth, and then keeps stable within 170 µm. On the other hands, with the smaller spot to spot distance of 0.5/0.5, the residual stress of the sample increases to -302.3 ± 24.6 MPa at 40 µm depth, and then keeps stable within 125 µm. It is observed that the decrease of the spot to spot

distance results in the increment of the peak residual stress, while the laser peening affected depth also increases according to the trend of the curve.

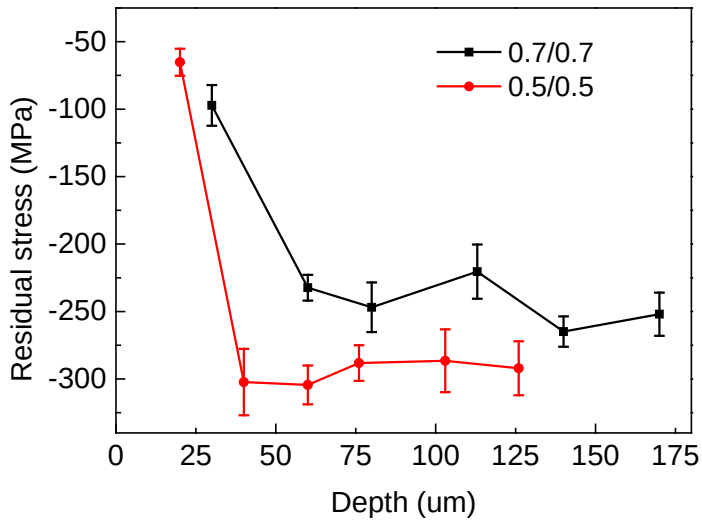

Fig. 51. In depth residual stress distribution of the 1018 CS after laser peening without coating with different spot to spot distances (1.4 mm spot diameter, 650 mJ pulse energy, 0.5/0.5 or 0.7/0.7 spot to spot distance, 1 time).

By comparing Fig. 50. and Fig. 51., the effect of the sacrificial coating (100 µm black tape) could be revealed. With the same parameters (650 mJ, 0.5/0.5 spot distance, 1 LSP impact), the peak residual stress values along the depth are almost the same no matter the black tape was used or not, while the peak compressive residual stress keeps stable in depth and could extend to deeper regions if the black tape is not employed.

2.2.2.4. Metallographic investigation on the 1018 CS surface

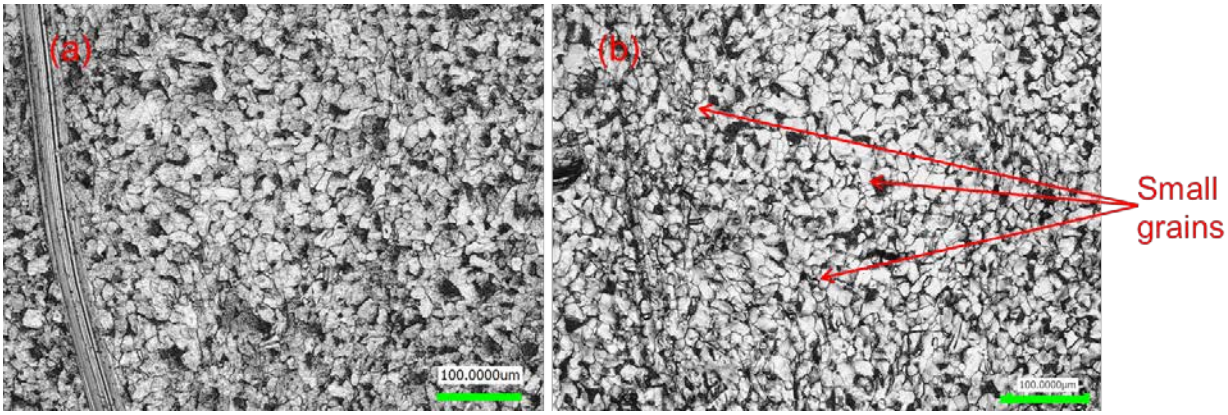

Fig. 52. Grain structure on the 1018 CS surface (a) before and (b) after laser peening with black tape (1.4 mm spot diameter, 650 mJ pulse energy, 0.5/0.6 spot to spot distance, 10 times)

The microstructure variation on the 1018 CS surface due to the laser shock peening with 100 µm black tape as the sacrificial coating (1.4 mm spot diameter, 650 mJ pulse energy, 0.5/0.6 spot to spot distance, 10 times) was investigated by metallographic imaging Fig. 52a and 52b show the two photos captured in the same region of the sample surface before and after laser peening, respectively. Tremendous small grains are observed after laser peening (Fig. 52b), while the grain size before LSP is much larger (Fig. 52a). The grain refinement due to LSP could further increase the resistance of the CS to stress corrosion cracking besides the generation of the compressive residual stress, which is due to the much more complicated grain boundaries with smaller grains.

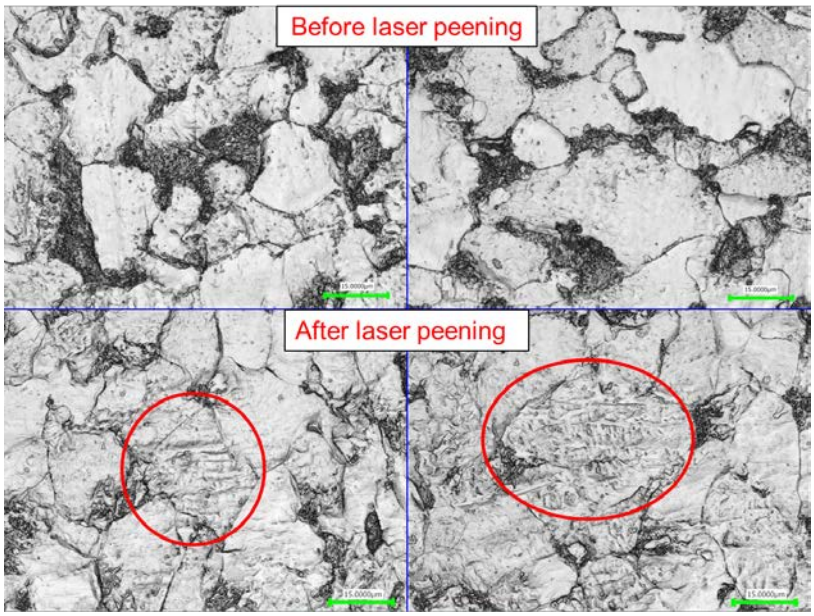

Fig. 53. Microstructure inside the grains on the 1018 CS surface before and after laser peening with black tape (1.4 mm spot diameter, 650 mJ pulse energy, 0.5/0.6 spot to spot distance, 10 times)

The structures inside the grains were also investigated by metallographic imaging. As shown in Fig. 53., serious slip bands could be observed in side some of the grains after laser peening, which could be barely found before laser peening. The generation of extra slip bands reflects the existing of high compressive residual stress.

The microstructure change on the 1018 CS surface due to the laser shock peening with 100 µm black tape as the sacrificial coating was further investigated by in-situ metallographic imaging. Fig. 54 shows three large area metallographic images captured in the similar region of one 1018 CS plate: (a) after polishing & etching; (b) after polishing & etching and laser peening; (c) after polishing & etching, laser peening, and re-polishing & re-etching. The grain structure could be observed obviously after polishing & etching, but it became obscure after laser peening. Therefore, electrochemical polishing and etching was performed again to show clear the microstructure change after laser peening. Since the time for electrochemical polishing and

etching was very short, the grain structure should remain the same for Fig. 54b and 54c. Comparing the large are imaging in Fig. 54a and 54c, slight grain refinement could be observed after laser peening.

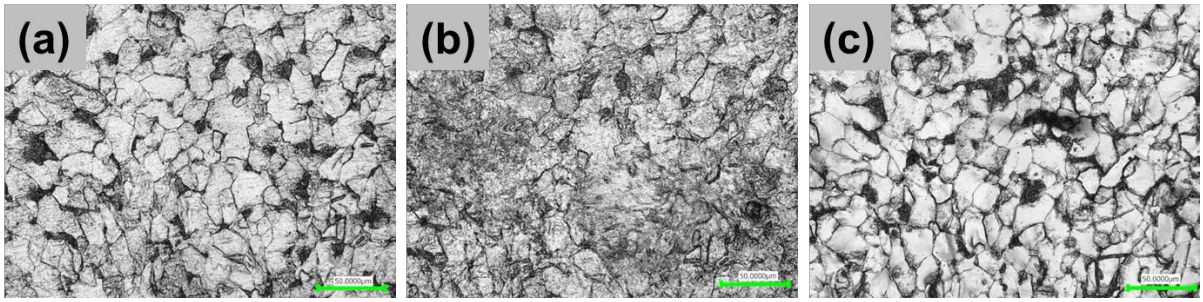

Fig. 54. Large area grain structure on the 1018 CS surface (a) before and (b)(c) after laser peening with black tape (1.4 mm spot diameter, 650 mJ pulse energy, 0.5/0.6 spot to spot distance, 10 times). (c) was captured after re-polishing and re-etching

To clarify the grain structure change, in-situ metallographic imaging was further performed in localized surface regions. In Fig. 55, specific grain structures were marked out by red profiles (a) before and (b) after laser peening. Comparing these structures, we could find extra grain boundaries inside the original grains, splitting the large grain into smaller ones, which explains the generation of the smaller grain and grain refinement phenomenon in Fig. 54.

In summary, both the large area and localized in-situ metallographic imaging revealed the grain refinement after laser peening, which could further increase the resistance of the CS to stress corrosion cracking due to the more complicated grain boundaries.

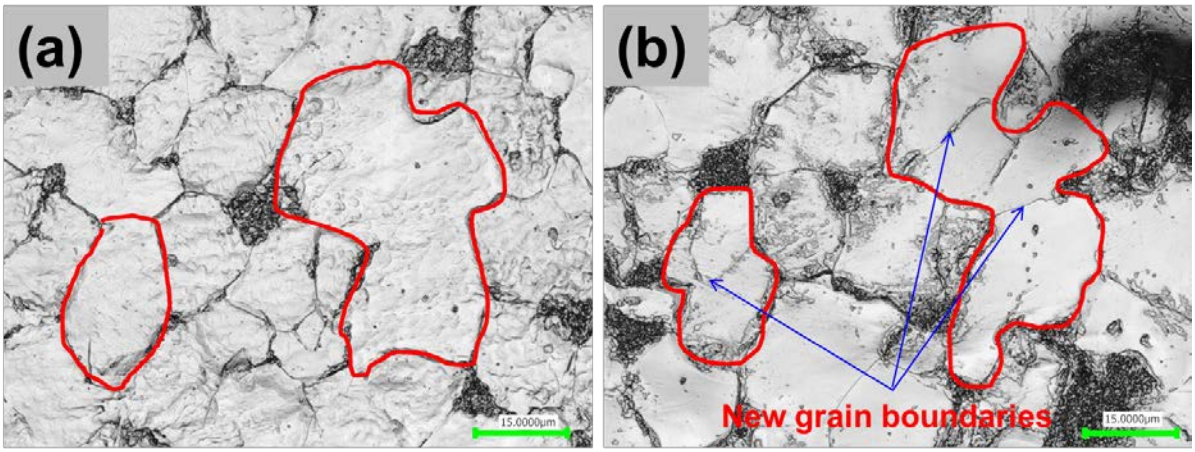

Fig. 55. In-situ grain structure change on the 1018 CS surface (a) before and (b) after laser peening with black tape (1.4 mm spot diameter, 650 mJ pulse energy, 0.5/0.6 spot to spot distance, 10 times). (b) was captured after re-polishing and re-etching

2.2.3. Portable laser shock peening equipment proposal and development

The above research results of this project have successfully demonstrated that laser shock peening technology can improve the corrosion resistance of pipeline steels, which will significantly improve the safety, reduce the environmental impacts, and enhance the reliability of the nation's pipeline transportation system. Therefore, the proposed in-lab laser peening system preliminary design is feasible and could be fabricated out, as shown in Fig. 56. As the in-lab laser peening system using high pulse energy (over 2 J) Nd:YAG laser, the whole laser peening system is relative expensive, bulky (system over 200 kg), and sensitive to the operating environments. Therefore, this system can only be installed in a fixed base such as workshop or laboratory, and the workpieces need to be transported to the workshop for laser peening before being shipped to the assembling sites.

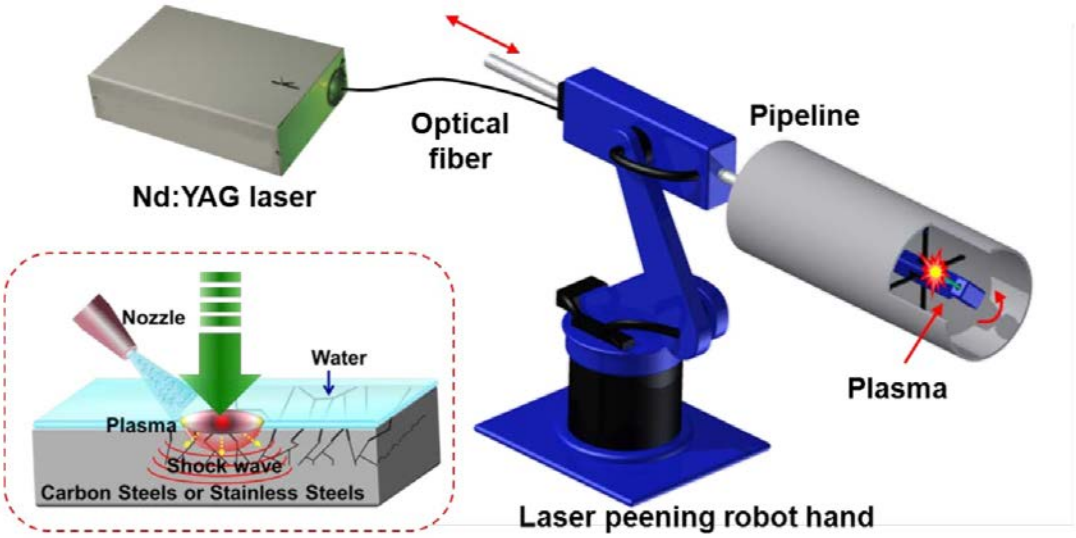

Fig. 56. Preliminary design of the in-lab laser peening equipment for pipeline system

However, if compact laser sources with low pulse energy could be used for peening and maintain comparable peening effects, all these shortcomings in laser peening can be overcame.

The PI's group has made a long-term effort to develop industrial low energy laser peening technology for Al-Mg alloy. With the support from Office of Naval Research (ONR), we have achieved over 200 MPa compressive stress layer (500~2000 μm depth) on Al-Mg alloy ship plate surface using a compact Nd:YAG laser with only 0.65 J pulse energy (Fig. 57 a&b). The peening process can be operated on site and demonstrated remarkable SCC resistance enhancement of ship plate. A portable laser peening system for on-site peening of ship plate was also designed and fabricated, as shown in Fig. 58 and Fig. 59.

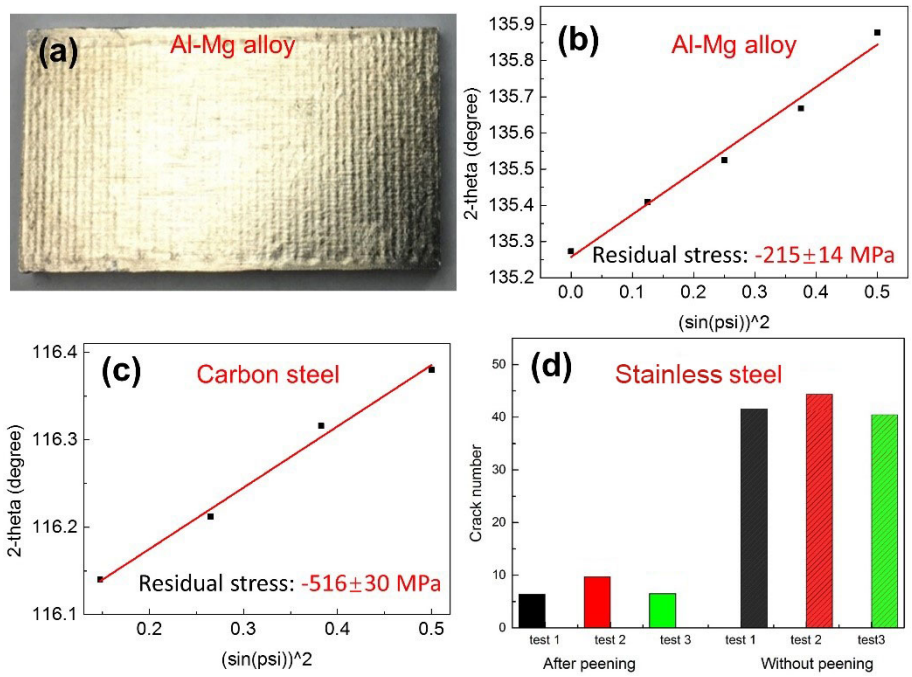

Fig. 57. Low energy laser peening research conducted by the PI's group. (a) & (b) Surface topography and residual stress of Al-Mg alloy surface after peening with 0.65 J laser pulse energy; (c) Residual stress and SCC test results of pipeline steels after peening with 0.85/0.65 J laser pulse energy.

The PI's group also successfully verified the feasibility of using low pulse energy laser to peen pipeline steels. By adopting some developed low energy laser peening technologies for Al-Mg ship plate, we observed comparable peening performance on pipeline steels by using laser pulse energy of only 0.85 J or 0.65 J, as well as SCC resistance improvement, as shown in Fig. 10 c&d.

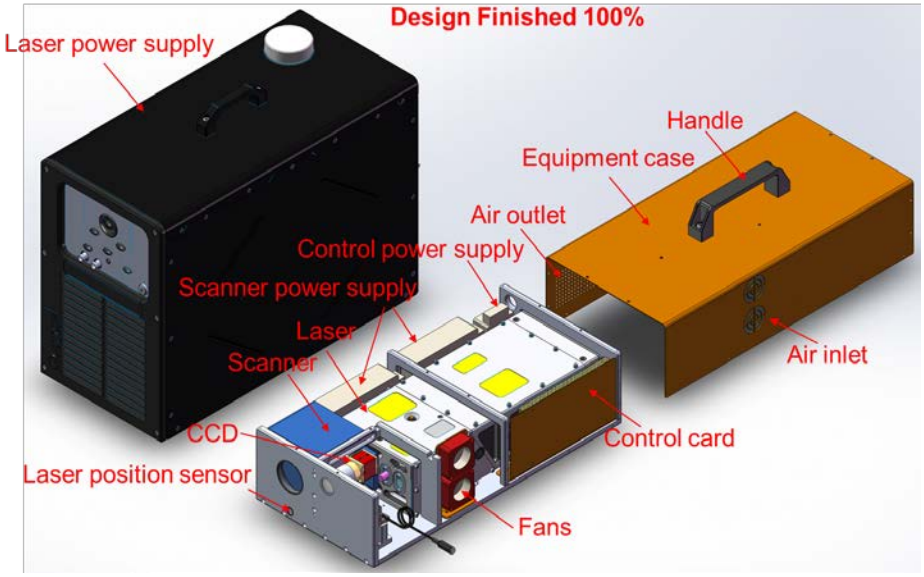

Fig. 58. Overall design of the portable laser peening system for Al-Mg ship plate

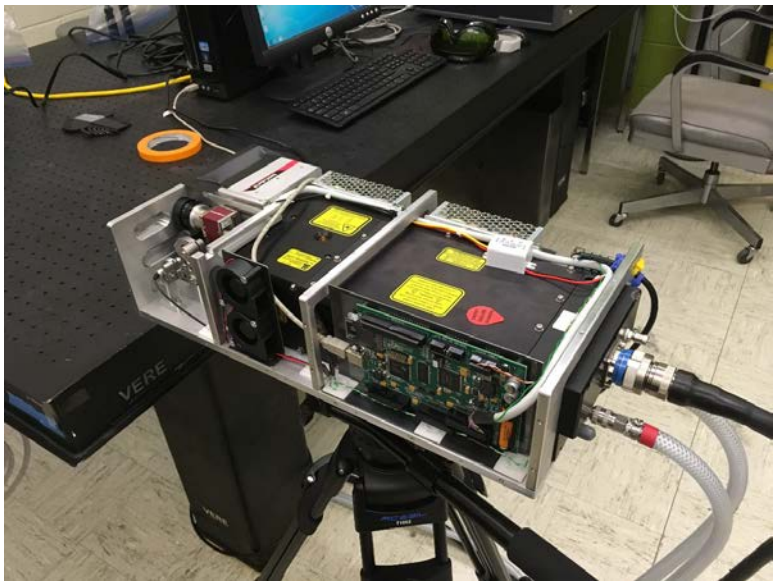

Fig. 59. Photo of the practical portable laser peening system under construction for ONR.

Thus, further studying the low energy laser peening technologies for pipeline steel and developing an on-site high speed laser peening equipment for pipeline industry are better solutions compared to the in-lab laser peening system developed in this project. Therefore, the PI's group submited a new proposal to DOT to apply fundings which can support the systematical investigation of the low energy laser peening technologies and make low energy laser peening technology industrially reliable for metalic pipeline. Most of all, a fully developed on-site high speed laser peening prototype will be provided for preventing pipeline corrosion.

The portable laser peening system supported by the Office of Naval Research (ONR) was under further design and modification, which is a meaningful prototype for future pipeline peening equipment to prevent stress corrosion cracking. The preliminary design of the portable laser peening system is consisted of a nanosecond Nd:YAG laser with a pulse energy of ~ 650 mJ, focus lens groups, beam delivery system, control system and power system. An adjustable lens group helps to control the focal plane. The beam delivery system could direct the beam to scan arbitrary shapes as programed, which works instead of the 3D stage and much more appropriate for in-field applications. Just as we stated for the in-lab setup, if the incident Nd:YAG laser beam emitted perpendicular on the sample surface, serious water jet and particles generated in the laser peening process tend to contaminate the optical system and shield subsequent laser pulse energy. Therefore, a small tilt angle was still adopted to irradiate the laser beam so that the contamination particles and water jet were prevented from reaching the optical system. The protective glass was used to guarantee the safety of the lens and mirrors. According to previous results, the laser repetition rate was still 5 Hz and the sacrificial layer was 100 μm black tape to reduce the shock wave attenuation in the sacrificial layer and enhance better peening effect. The focus position was carefully optimized by comparing morphology changes after laser peening at

different positions.

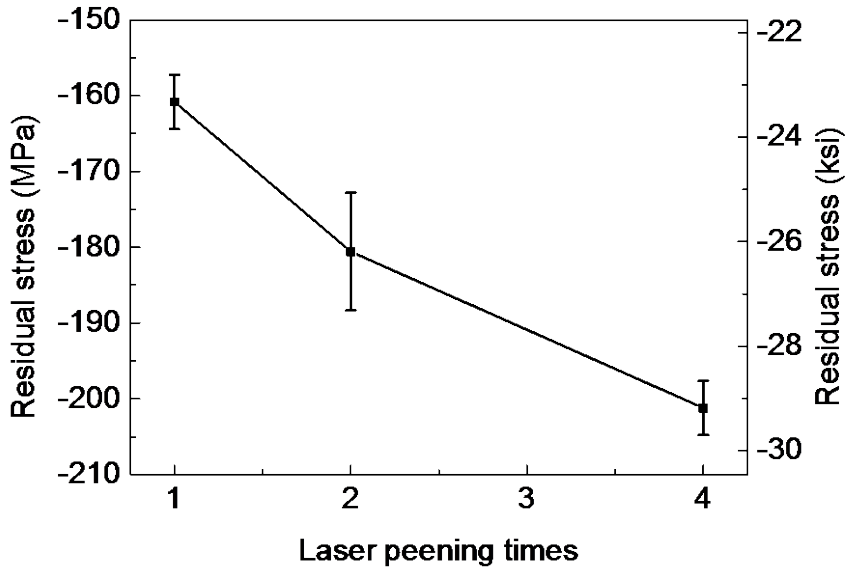

Fig. 60. Surface residual stress of Al alloy after portable Nd:YAG laser peening (~2.5 mm spot diameter after focusing, 650 mJ pulsed energy, 1/2/4 LSP times, 70% overlap rate, 100 μm black tape).

Fig. 60. shows the surface residual stress of Al alloy samples after laser shock peening by the portable system for different times with an overlapping rate of 70 %. A 100 μm black tape is used as the sacrificial layer and replace after each peening process. The lens group used in the portable peening system is limited in sized so that it could only focus the laser spot to a ~2.5 mm diameter. However, even though the spot size is very large, the surface residual stress could still reach -160 MPa (-23.2 ksi) after only 1 laser peening impact. Moreover, the residual stress increases with the increment of the laser peening times. After 4 LSP impacts, the residual stress could increase to over -200 MPa (-29 ksi), which is comparable with previous results. On the other hand, due to the large spot size, which makes the shock wave harder to attenuate, the residual stress could be distributed even deeper than that obtained with smaller spots. After modification of the laser with the help of the manufacturer, the residual stress could be further improved in future researches.

2.3. Key outcomes

In this project, laser shock peening and laser cleaning techniques were researched to examine their capability for improving the corrosion resistance of pipeline steel against failure. The major achievements and conclusions have been summarized as follows:

(1) Laser cleaning system was established with Nd:YAG lasers, which was used for the cleaning of mixed coatings (mixture of rubber, paint and high temperature resistant coating), black tape, and transparent resin. The mixed coatings and black tape could be cleaned without

causing any surface damage on sample surfaces, while the transparent resin was removed with a little increase in surface roughness.

(2) High-energy LSP system was developed with a Continuum Nd:YAG laser. The effect of laser pulse energy, wavelength, repitition rate, impact times, overlapping rate, sacrificial layer material/structure, and water flow control was investigated and optimized. The nanohardness and microhardness were observed to increase obviously after LSP and gradient hardness distribution on the surface and along depth was also measured on 304 SS and CS. Metallographic imaging indicates grain refinement in both 304 SS and CS, which is not obvious. TEM investigation shows the increase of defects such as dislocations, stacking faults, and twins in 304 SS. SCC tests show intergranular craking in 304 SS and obvious decrease was observed in crack numbers on the laser peened surfaces. In all, the high energy LSP system shows the ability to incrase the mechanical and corrosion properties of pipeline steels due to the microstructure changes.

(3) Low-energy LSP system was developed with a Quantel Nd:YAG laser. The technique shows similar effects as the high-energy LSP, which can increase the surface and in-depth compressive residual stress and induce grain refinement of 1018 CS. LSP without sacrificial coating was also tested with the system, showing sharp change from tensile stress on the surface and compressive stress along depth.

(4) Based on the above studies, a portable LSP system was proposed and the preliminary design and tests show promising results, which need further supports for further design modifications and practical tests.

3. Description of any risks/challenges

No risks were experienced in this project.

4. Future researches related to this project

The specific modification of the portable LSP system for pipeline usage, in-site tests, and further design improvements.